

Maximum Electromagnetic Local Density of States via Material Structuring

Pengning Chao,^{1,*} Rodrick Kuate Defo,^{1,*} Sean Molesky,² and Alejandro Rodriguez¹

¹*Department of Electrical and Computer Engineering,
Princeton University, Princeton, New Jersey 08544, USA[†]*

²*Department of Engineering Physics, Polytechnique Montréal, Montréal, Québec H3T 1J4, Canada*
(Dated: October 4, 2022)

The electromagnetic local density of states (LDOS) is crucial to many aspects of photonics engineering, from enhancing emission of photon sources to radiative heat transfer and photovoltaics. We present a framework for evaluating upper bounds on the LDOS in structured media that can handle arbitrary bandwidths and accounts for critical wave scattering effects. The bounds are solely determined by the bandwidth, material susceptibility, and device footprint, with no assumptions on geometry. We derive an analytical expression for the maximum LDOS consistent with the conservation of energy across the entire design domain, which upon benchmarking with topology-optimized structures is shown to be nearly tight for large devices. Novel scaling laws for maximum LDOS enhancement are found: the bounds saturate to a finite value with increasing susceptibility and scale as the quartic root of the bandwidth for semi-infinite structures made of lossy materials, with direct implications on material selection and design applications.

INTRODUCTION

The electromagnetic local density of states (LDOS), a measure of local response—the electric field from a dipolar current source—at a given point in space [1], plays a central role in many nanophotonic phenomena and applications, including spontaneous [2] and stimulated [3] emission, quantum information [4], surface enhanced Raman scattering [5, 6], photovoltaics [7], radiative heat transfer [8], non-linear frequency conversion [9], scintillation [10], to name a few. Enhancing the LDOS by nanostructuring bulk media, a persistent theme in photonics design, is often achieved through the creation of optical resonances [11]: a cavity or resonator supporting a single mode of quality factor Q and mode volume V enhances the LDOS in proportion to the Purcell factor Q/V . Many classic design schemes rely on maximizing Q (ring resonators [12]), minimizing V (plasmonic nanocavities [13, 14], bow-tie antennae [15]), or a combination thereof (photonic crystal cavities [16], metal-dielectric hybrid structures [17]). Going beyond the single mode picture, multi-mode and dispersion-based effects such as exceptional points [18, 19] and slow light devices [20] have also been explored. Recently, complex devices obtained by application of large-scale structural optimization appear to combine several confinement mechanisms [21, 22], providing further improvements on device performance.

Given its relevance in optics and the ever increasing structural freedom brought on by advances in nanofabrication [23], interest in assessing limits on achievable LDOS enhancement has grown over the past few decades [24]. Spectral sum rules [25–27] pin the frequency-integrated LDOS of any system but are of limited utility in practical settings involving finite and often narrow source bandwidths. Specialized results pertaining to achievable mode quality factors [28] or mode volumes in cavity settings [29] have proven useful in many applications but

are not sufficiently general to account for multi-mode effects. Passivity requirements based on achievable material response were recently used to bound both single-frequency [30] and finite-bandwidth [31] LDOS. However, passivity alone cannot fully capture the wave nature of light as constrained by Maxwell’s equations, e.g., the necessity of phase matching to achieve resonance, leading to loose limits when contributions other than those coming from evanescent fields become relevant.

In this article, we generalize and lift several limitations imposed by these prior approaches to provide expressions and predictions for the largest spectral-integrated LDOS that may be achieved in a structured medium. The derived bounds incorporate wave and material constraints imposed by Maxwell’s equations over any desired length-scale and are geometry agnostic: besides specifying the material susceptibility χ , a frequency window of interest, and a bounding domain that the structured medium must reside within, no further assumptions are made on device topology. We consider sources both enclosed within and external to devices, obtaining bounds that generally come within an order of magnitude of complicated structures discovered through inverse methods [32]. Furthermore, we find that the mere requirement of energy conservation is sufficient to place tight limits on large devices; we exploit this fact to derive an analytical upper bound (13) along with integral expressions and asymptotic analysis for the particular scenario of a source above a semi-infinite, structured slab. The bounds show saturation to a finite value as $\chi \rightarrow \infty$ and varying power-law scalings with respect to source bandwidth $\Delta\omega$, with the maximum LDOS transitioning from a scaling $\propto \Delta\omega^{-1}$ to one $\propto \Delta\omega^{-1/4}$ as material absorption begins to limit the net enhancement that any one mode may contribute.

PROBLEM FORMULATION

Working in dimensionless units of $\epsilon_0 = \mu_0 = 1$, and considering only nonmagnetic materials, the partial LDOS at frequency ω and position \mathbf{x}' along the direction $\hat{\mathbf{e}}$ can be shown to be, by Poynting's theorem [33], directly proportional to the average power $\rho(\omega)$ emitted by a harmonic dipole source $\mathbf{J}(\mathbf{r})e^{-i\omega t} = e^{-i\omega t}\delta(\mathbf{x} - \mathbf{x}')\hat{\mathbf{e}}$ at the same location,

$$\rho(\omega) \equiv -\frac{1}{2} \text{Re} \left\{ \int \mathbf{J}^*(\mathbf{r}) \cdot \mathbf{E}(\mathbf{r}) d\mathbf{r} \right\} \quad (1)$$

where the electric field generated by the \mathbf{J} solves Maxwell's equations,

$$\nabla \times \nabla \times \mathbf{E}(\mathbf{r}) - \omega^2 \epsilon(\mathbf{r}) \mathbf{E}(\mathbf{r}) = i\omega \mathbf{J}(\mathbf{r}). \quad (2)$$

Since real sources emit light over a finite bandwidth (e.g., the Planck spectrum of heated bodies or fluorescence/spontaneous emission linewidth of atoms [34]), we instead consider the more natural choice of a frequency average of $\rho(\omega)$ over a Lorentzian lineshape centered at ω_0 with bandwidth $\Delta\omega_{src} = \omega_0/2Q_{src}$ (corresponding source “quality factor” Q_{src}):

$$\langle \rho \rangle_{\omega_0, Q_{src}} = \int_{-\infty}^{\infty} \frac{\Delta\omega_{src}/\pi}{(\omega - \omega_0)^2 + \Delta\omega_{src}^2} \rho(\omega) d\omega, \quad (3a)$$

As pointed out in [32], such a modified figure of merit not only captures the spectral lineshape of many practical sources [34], but also offers a computational and conceptual advantage: instead of evaluating the frequency integral in (3a) directly, one can instead carry out a complex- ω contour integral over the upper half plane and exploit causality to convert, using the residue theorem, the spectral average $\langle \rho \rangle$ to the single complex-frequency $\rho(\tilde{\omega})$ and an electrostatic (zero-frequency) contribution:

$$\langle \rho \rangle_{\omega_0, Q_{src}} = \rho \left(\tilde{\omega} \equiv \omega_0 + \frac{\omega_0}{2Q_{src}} i \right) + \frac{4Q_{src}}{\pi(4Q_{src}^2 + 1)\omega_0} \alpha. \quad (4)$$

Here $\alpha = \frac{1}{2} \text{Re}\{\mathbf{p}_0 \cdot \mathbf{E}_0\}$, where \mathbf{p}_0 is a unit amplitude electrostatic dipole and \mathbf{E}_0 the field it generates; this electrostatic contribution leads to an all-frequency integrated sum rule in the wide bandwidth limit [27, 31]. In this paper we will be focusing on the practically important case of moderate or narrow source bandwidth with $Q_{src} \gg 1$ and thus will neglect the electrostatic term in (4) going forward.

Thus, the structural design problem for maximizing bandwidth-averaged LDOS can be formulated as

$$\max_{\epsilon(\mathbf{r}; \tilde{\omega})} \rho(\tilde{\omega}) = -\frac{1}{2} \text{Re} \left\{ \int \mathbf{J}^*(\mathbf{r}; \tilde{\omega}) \cdot \mathbf{E}(\mathbf{r}; \tilde{\omega}) d\mathbf{r} \right\} \quad (5a)$$

given the constraints

$$\nabla \times \nabla \times \mathbf{E}(\mathbf{r}; \tilde{\omega}) - \tilde{\omega}^2 \epsilon(\mathbf{r}; \tilde{\omega}) \mathbf{E}(\mathbf{r}; \tilde{\omega}) = i\tilde{\omega} \mathbf{J}(\mathbf{r}; \tilde{\omega}) \quad (5b)$$

$$\epsilon(\mathbf{r}; \tilde{\omega}) = \begin{cases} 1 \text{ or } 1 + \chi(\tilde{\omega}) & \mathbf{r} \in V \\ 1 & \mathbf{r} \notin V \end{cases} \quad (5c)$$

where V is a pre-specified design region that the structure resides within and $\chi(\tilde{\omega})$ the Fourier transform of the bulk material susceptibility evaluated at complex frequency $\tilde{\omega}$. In later expressions we may suppress the $\tilde{\omega}$ dependence of time-harmonic variables for notation simplicity.

Due to the high dimensionality of the structural degrees of freedom $\epsilon(\mathbf{r})$ and the non-convex dependence of the field $\mathbf{E}(\mathbf{r})$ on $\epsilon(\mathbf{r})$, it is generally not possible to solve for the global optimum of (5c) [35]. However, it is possible to exploit an alternative parametrization of the problem in which the polarization density $\mathbf{P}(\mathbf{r}) = (\epsilon(\mathbf{r}) - 1)\mathbf{E}(\mathbf{r})$ rather than $\epsilon(\mathbf{r})$ serve as optimization degrees of freedom, to obtain bounds on $\rho(\tilde{\omega})$ applicable to *any possible structure*, given only the choices of design region V and material susceptibility χ [24]. In this context, it becomes convenient to decompose the total field into the vacuum field emitted by the source and scattered field emitted by the polarization currents:

$$\begin{aligned} \mathbf{E}(\mathbf{r}) &= \mathbf{E}_{vac}(\mathbf{r}) + \mathbf{E}_{sca}(\mathbf{r}) \\ &= \frac{i}{\tilde{\omega}} \int \mathbb{G}(\mathbf{r}, \mathbf{r}') \cdot \mathbf{J}(\mathbf{r}') d\mathbf{r}' + \int \mathbb{G}(\mathbf{r}, \mathbf{r}') \cdot \mathbf{P}(\mathbf{r}') d\mathbf{r}' \end{aligned} \quad (6)$$

with $\mathbb{G}(\mathbf{r}, \mathbf{r}')$ denoting the vacuum dyadic Green's function, the solution to

$$\nabla \times \nabla \times \mathbb{G} - \tilde{\omega}^2 \mathbb{G} = \tilde{\omega}^2 \mathbb{I}. \quad (7)$$

Note that our definition of the Green's function has an extra global factor of $\tilde{\omega}^2$ compared to the standard definition. Similarly, the net power extracted from the dipole source can be decomposed into constant (structure-independent) vacuum and scattered-field contributions:

$$\rho = \rho_{vac} + \rho_{sca}(\mathbf{P}), \quad (8a)$$

$$\rho_{vac} = -\frac{1}{2} \text{Re} \left\{ \frac{i}{\tilde{\omega}} \iint \mathbf{J}^*(\mathbf{r}) \cdot \mathbb{G}(\mathbf{r}, \mathbf{r}') \cdot \mathbf{J}(\mathbf{r}') d\mathbf{r}' d\mathbf{r} \right\}, \quad (8b)$$

$$\begin{aligned} \rho_{sca}(\mathbf{P}) &= -\frac{1}{2} \text{Re} \left\{ \iint \mathbf{J}^*(\mathbf{r}) \cdot \mathbb{G}(\mathbf{r}, \mathbf{r}') \cdot \mathbf{P}(\mathbf{r}') d\mathbf{r}' d\mathbf{r} \right\} \\ &= \frac{1}{2} \text{Im} \left\{ \tilde{\omega} \int \mathbf{E}_{vac}(\mathbf{r}') \cdot \mathbf{P}(\mathbf{r}') d\mathbf{r}' \right\}, \end{aligned} \quad (8c)$$

where in the second line of (8c) we made use of the fact that $\mathbf{J}^* = \mathbf{J}$ (the global phase of dipole source is irrelevant) and the reciprocity relation $\mathbb{G}(\mathbf{r}, \mathbf{r}') = \mathbb{G}^T(\mathbf{r}', \mathbf{r})$. They key to formulating a shape-independent bound on ρ

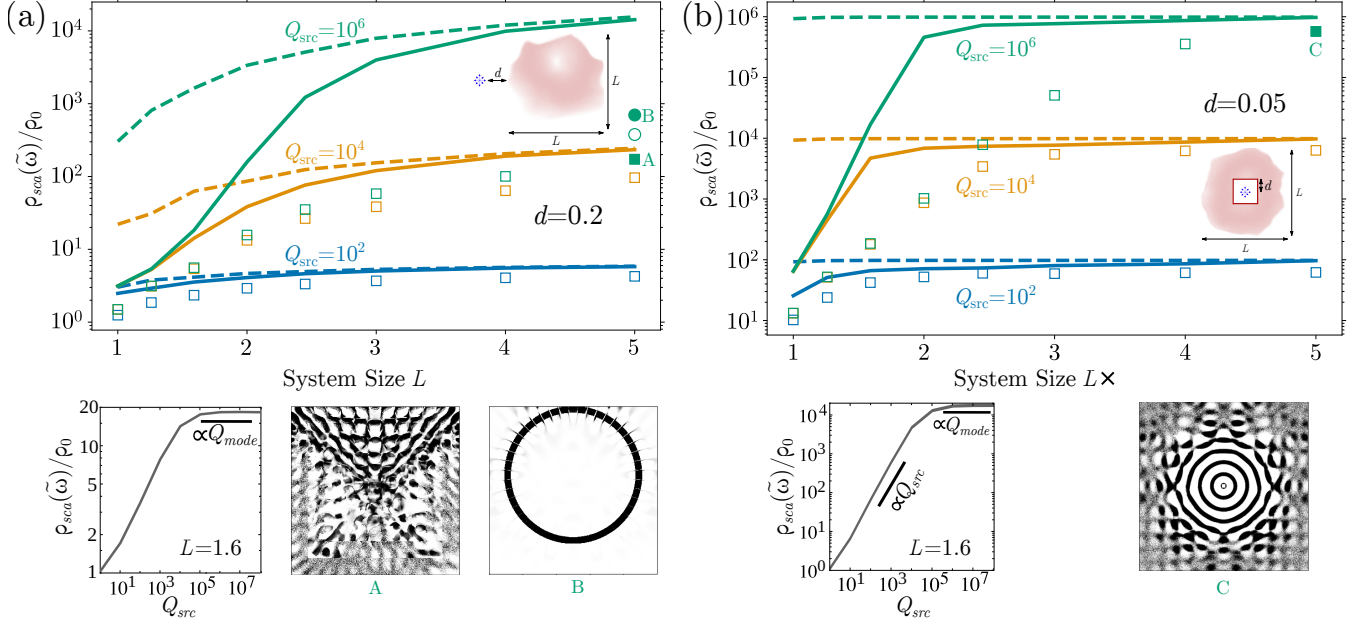


Figure 1. Bounds and inverse designs with TM polarization, $\chi = 4$, $Q_{src} \in \{10^2, 10^4, 10^6\}$, and finite design domain size L for (a) dipole on the side of a square design region and (b) dipole in the center of a square design region. Solid lines are bounds that are converged with respect to increasing the number of constraint subregions V_k . Dotted lines are bounds with just the global constraint $V_k = V$. Squares are topology optimized structures from random initializations. The hollow circle is a ring resonator with inner and outer radii approximately 1.85 and 2.05 respectively, with the exact resonant radius requiring accuracy up to 8 significant figures to achieve the plotted enhancement (SI); the filled circle is a topology optimized structure starting from that ring resonator. LDOS enhancement as a function of Q_{src} for fixed $L = 1.6$ is shown beneath the main figures, along with designs corresponding to filled shapes.

is to forgo the need for structural information by relaxing the requirement that \mathbf{P} satisfy Maxwell's equations everywhere, imposing instead a smaller subset of wave constraints [24]. Such constraints can be indeed be derived from Maxwell's equations through a complex frequency generalization of the time-harmonic Poynting's theorem (see [24] and SI), giving

$$\int_{V_k} \mathbf{E}_{vac}(\mathbf{r}) \cdot \mathbf{P}(\mathbf{r}) d\mathbf{r} = \int_V \mathbf{P}^*(\mathbf{r}) \cdot \int_{V_k} \mathbf{U}(\mathbf{r}, \mathbf{r}') \cdot \mathbf{P}(\mathbf{r}') d\mathbf{r}', \quad (9)$$

$$\mathbf{U} \equiv \chi^{*-1} \delta(\mathbf{r} - \mathbf{r}') - \mathbb{G}^*(\mathbf{r}, \mathbf{r}')$$

where $V_k \subseteq V$ is any spatial region within the design domain V and we have defined the composite operator \mathbf{U} . Notably, (9) can be interpreted as a statement of the conservation of energy over each spatial region, requiring only specification of the allotted design footprint V and available susceptibility χ . Note also that geometric information is contained only implicitly in \mathbf{P} , with material properties specified by the known complex scalar χ . The resulting optimization problem for the LDOS can be written as

$$\max_{\mathbf{P}(\mathbf{r}; \tilde{\omega})} \rho_{sca} = -\frac{1}{2} \text{Im}\{\tilde{\omega} \langle \mathbf{E}_{vac}^* | \mathbf{P} \rangle\} \quad (10a)$$

such that $\forall V_k \subseteq V$

$$\text{Re}, \text{Im} \{ \langle \mathbf{E}_{vac} | \mathbb{I}_{V_k} | \mathbf{P} \rangle - \langle \mathbf{P} | \mathbb{U} | \mathbb{I}_{V_k} | \mathbf{P} \rangle \} = 0 \quad (10b)$$

where \mathbb{I}_{V_k} is the projection operator into the region V_k . Above, we employed Dirac bra-ket notation for brevity, with $|\mathbf{a}\rangle$ denoting the vector field $\mathbf{a}(\mathbf{r})$ over the design domain V , $\langle \mathbf{a} | \mathbf{b} \rangle = \int_V \mathbf{a}^*(\mathbf{r}) \cdot \mathbf{b}(\mathbf{r}) d\mathbf{r}$ is the conjugated inner product, and operator action $\mathbb{A}|\mathbf{a}\rangle = \int_V \mathbb{A}(\mathbf{r}, \mathbf{r}') \cdot \mathbf{a}(\mathbf{r}') d\mathbf{r}'$. (10) is a quadratically constrained linear program for \mathbf{P} . While direct optimization is still not guaranteed to find a global optimum due to the non-convexity of certain constraints in (10b), a bound on the problem can be computed efficiently via the Lagrange dual function [24, 36, 37], hereby referred to as the dual bound.

In principle, the maximum LDOS achievable in a structured medium is known to grow indefinitely in the single-frequency limit of $\Delta\omega_{src} \rightarrow 0$. For instance, in lossless media, the whispering gallery modes of ring resonators and defect modes of photonic crystals exhibit exponential scaling in Q with increasing system size [16, 38], while their mode volumes either increase polynomially or remain constant, respectively, leading to exponential growth in the Purcell factor. Geometries with sharp tips can also give rise to field singularities and hence vanishing mode volumes [39]. However, in practice, finite source bandwidths, device footprint, and material losses limit

the utility of diverging lifetimes, while fabrication imperfections and atomic-scale effects preclude realization of arbitrarily small features. As will be seen below, the imposition of finite $\Delta\omega_{src}$ and a minimum vacuum gap d between source and medium regularizes such divergences, paving the way for investigations of LDOS growth characteristics in realistic settings. We also note that for finite $\Delta\omega_{src}$ the vacuum LDOS contribution ρ_{vac} diverges due to contributions from high frequencies. This is an artifact of the Lorentzian lineshape chosen and has little bearing on practical applications; the results presented will thus focus on the structural contribution ρ_{sca} which does remain finite.

To make explicit the scale invariance of Maxwell's equations, all lengths are given in units of the center wavelength $\lambda_0 = 2\pi c/\omega_0$ and ρ_{sca} normalized by the single-frequency vacuum dipole radiation $\rho_0 \equiv \rho_{vac}(\omega_0)$.

NUMERICAL RESULTS

The dual bound can be obtained numerically for arbitrary domains via a suitable representation of the Green's function and Maxwell operator. We do so for two standard settings: an external-dipole configuration where the dipole is adjacent to the structure, relevant for instance to gratings and solid-state defect couplers [40, 41]; and an enclosed-dipole configuration in which the dipole is surrounded by the structure, relevant to photonic crystal cavities [16], bullseye gratings [42], and bowtie antennas [15]. For computational convenience, all calculations are performed in 2d for both the out-of-plane (scalar) TM and in-plane (vectorial) TE electric-field polarizations. The finite-difference frequency-domain method is used to represent all relevant fields and operators (SI). Progressively tighter bounds were obtained by gradually increasing the number of constraint sub-regions V_k down to the computational pixel level. Inverse designs were also obtained to compare against the bounds, following the topology optimization (TO) approach detailed in [32].

Results pertaining to maximum LDOS for both external and enclosed configurations are shown in Figure 1 as a function of the design footprint. Since the vacuum LDOS diverges when integrated against a Lorentzian lineshape [25, 31, 32], this and subsequent results pertain only to the structural contribution ρ_{sca} , defining the enhancement factor in relation to the single-frequency vacuum emission $\rho_0 \equiv \rho_{vac}(\omega_0)$. In both settings the medium is assumed to be lossless, $\text{Im } \chi = 0$. For a fixed Q_{src} , the bounds are seen to grow exponentially before saturating with increasing domain size L . Conversely, for fixed L the bounds grow linearly before saturating with increasing Q_{src} . Both observations are consistent with a resonant enhancement mechanism: since the finite vacuum gap d precludes field divergences in the vicinity of the dipole, thereby imposing an upper bound on its cou-

pling to any mode, one would expect improvements in the Purcell factor to be mainly driven by growth in the modal lifetimes. Supposing a system with response dominated by a single mode of quality factor $Q_{mode} = \omega_0/2\Delta\omega_{mode}$, (3a) yields a frequency-integrated LDOS that scales as

$$\int_{-\infty}^{\infty} \frac{\Delta\omega_{src}/\pi}{\omega^2 + \Delta\omega_{src}^2} \frac{\Delta\omega_{mode}/\pi}{\omega^2 + \Delta\omega_{mode}^2} d\omega = \frac{Q_{src}Q_{mode}}{2\pi\omega_0(Q_{src} + Q_{mode})}. \quad (11)$$

Thus, this modal picture predicts linear growth $\propto Q_{src}$ in (3a) so long as the system supports a sufficiently long-lived mode, $Q_{mode} \gg Q_{src}$, eventually saturating to a value $\propto Q_{mode}$ whenever $Q_{mode} \ll Q_{src}$. In the absence of material dissipation, the highest achievable Q_{mode} is constrained solely by radiative losses and, as confirmed by our bound calculations, known to scale at least exponentially with L in ring-resonator and photonic-crystal cavities. Comparing our bounds (solid lines) against inverse designs (squares), one observes remarkable alignment, with bounds and designs often coming within an order of magnitude of each other. The biggest performance gaps occur at high Q_{src} in the external configuration and can at least be partially attributed to TO getting trapped in local optima that, regardless of exhaustive initial conditions, underperform simple ring resonator geometries. Even starting with ring resonators as initial seeds, TO was only able to make modest improvements. In contrast, Bragg-onion type structures discovered by TO in the cavity setting are seen to tightly approach corresponding bounds. Comparing the high degree of precision needed to specify the dimensions of the ring resonator against the relative robustness of photonic bandgap confinement [43], we hypothesize that attaining high-performing designs for the external configuration at narrow bandwidths requires resonances based on sensitive interference cancellation. This leads to an ill-behaved optimization landscape with many subpar local optima to get stuck in, with ring resonators as an example of a class of high-performing designs not easily discoverable via brute-force optimization.

Finally, the observed dependence of the dual bound on the number and size of subregion constraints (10b) reveals two important features: first, the necessity of imposing many subwavelength constraint regions (SI) for the bounds to exhibit saturation as $Q_{src} \rightarrow \infty$; second, the fact that a single, global energy-conservation constraint appears sufficient to produce tight bounds when either device sizes or source bandwidths become sufficiently large. This suggests that subregion constraints are necessary to adequately “resolve” wave effects, including phase-matching restrictions, that limit mode confinement in finite systems; conversely, when system sizes no longer limit the highest achievable Q_{mode} in relation to Q_{src} , the latter and not the former becomes a bottleneck for further enhancements.

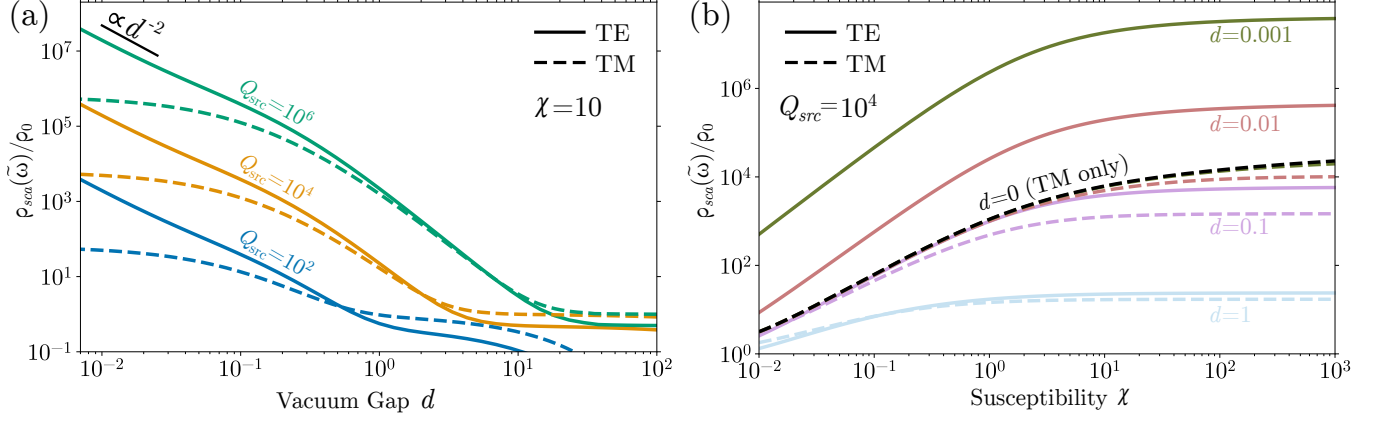


Figure 2. Maximum LDOS enhancement near a half-space design region as a function of (a) separation distance and (b) real material susceptibility χ for lossless dielectrics. While (b) plots bounds for lossless dielectrics, the material independent limit as $\chi \rightarrow \infty$ is a bound for general lossy χ as well (SI).

LARGE-SIZE SEMI-ANALYTICS

We now exploit the remarkable success of global energy conservation in describing large system behavior to obtain a semi-analytical bound on the maximum LDOS above a semi-infinite structure, i.e., the $L \rightarrow \infty$ limit of the external-dipole configuration depicted in Figure 1a. As shown in SI, the solution of the dual problem under both resistive and reactive energy conservation constraints (10b) can be mapped to a family of solutions involving a unitary phasor parametrized by the single constraint angle θ , leading to the modified problem:

$$\max_{\mathbf{P}(\mathbf{r};\tilde{\omega})} \rho_{sca} = -\frac{1}{2} \text{Im}\{\tilde{\omega} \langle \mathbf{E}_{vac}^* | \mathbf{P} \rangle\} \quad (12a)$$

such that for $\mathbf{P} \in V$,

$$\text{Im}\{e^{i\theta} \langle \mathbf{E}_{vac} | \mathbf{P} \rangle\} - \langle \mathbf{P} | \text{Asym}(e^{i\theta}\mathbb{U}) | \mathbf{P} \rangle = 0 \quad (12b)$$

where $\text{Asym}(\mathbb{A}) = (\mathbb{A} - \mathbb{A}^\dagger)/2i$ is the Hermitian anti-symmetric component of the operator \mathcal{A} . Owing to its simplicity, the solution to this dual bound for any given

θ can be written explicitly as

$$\rho_{sca} \leq \frac{1}{4} \text{Re}\left\{ \left(-\tilde{\omega}^* e^{i\theta} |\mathbf{E}_{vac}^*\rangle + |\tilde{\omega}| |\mathbf{E}_{vac}\rangle \right)^\dagger \text{Asym}(e^{i\theta}\mathbb{U})^{-1} |\mathbf{E}_{vac}\rangle \right\}, \quad (13)$$

which notably, depends only on the analytically known quantities \mathbf{E}_{vac} , χ , and \mathbb{U} . The tightest dual bound consistent with (13) can thus be obtained numerically by carrying out an additional optimization over θ , restricted so that $\text{Asym}(e^{i\theta}\mathbb{U})$ is positive definite (SI). Further analytical insight can be gleaned by expanding the operators and fields in a spectral basis conforming to the symmetry of the design domain: for a half-space enclosure, the natural choice is a Fourier basis $e^{ik_{\parallel}x_{\parallel}}$ parametrized by the wavevector k_{\parallel} parallel to the half-space surface. Carrying out this expansion for the incident field $|\mathbf{E}_{vac}\rangle$ yields,

$$|\mathbf{E}_{vac}\rangle = -\frac{\tilde{\omega}}{2\sqrt{2\pi}} \int_{-\infty}^{\infty} \frac{e^{ik_{\parallel}x_{\parallel}}}{\sqrt{2\pi} k_{\perp}} e^{ik_{\perp}x_{\perp}} e^{ik_{\perp}d} dk_{\parallel} \quad (14a)$$

where $k_{\perp} = \sqrt{\tilde{\omega}^2 - k_{\parallel}^2}$ and $\text{Im}(k_{\perp}) \geq 0$. For each conserved k_{\parallel} , the inverse operator image $\text{Asym}(e^{i\theta}\mathbb{U})_{k_{\parallel}}^{-1} \cdot e^{ik_{\perp}x_{\perp}}$ can be similarly expanded and evaluated explicitly as the sum of two complex sinusoids, leading to

$$\rho_{sca} \leq \min_{\theta} \frac{1}{16\pi} \int_0^{\infty} \text{Re}\left\{ -\frac{\tilde{\omega}^3 e^{i\theta} e^{2ik_{\perp}d}}{k_{\perp}^2} \left[\frac{R_1}{r_1 - ik_{\perp}} + \frac{R_2}{r_2 - ik_{\perp}} \right] + \frac{|\tilde{\omega}|^3 e^{-2\text{Im}(k_{\perp})d}}{|k_{\perp}|^2} \left[\frac{R_1}{r_1 + ik_{\perp}^*} + \frac{R_2}{r_2 + ik_{\perp}^*} \right] \right\} dk_{\parallel} \quad (15)$$

where the closed-form complex coefficients $R_{1,2}(k_{\parallel};\theta)$ and decay constants $r_{1,2}(k_{\parallel};\theta)$ are given in the SI.

The main challenge in evaluating (13) comes from the need to compute the inverse image of $\text{Asym}(e^{i\theta}\mathbb{U}) =$

$[\text{Im}\{e^{i\theta}/\chi^*\} + \text{Asym}(e^{-i\theta}\mathbb{G})]^{-1}$, which contains constraints on wave propagation via its dependence on the vacuum Green's function \mathbb{G} . In that regard, it is useful to consider an expansion of (13) in orders of $\text{Asym}(e^{-i\theta}\mathbb{G})$ (after using the Cauchy-Schwartz inequality to relax the term involving \mathbf{E}_{vac}^* (SI)):

$$\begin{aligned} \langle \rho \rangle_{max} &= \frac{|\tilde{\omega}|}{2} \langle \mathbf{E}_{vac} | \left[\text{Im}\left\{ \frac{e^{i\theta}}{\chi^*} \right\} + \text{Asym}(e^{-i\theta}\mathbb{G}) \right]^{-1} | \mathbf{E}_{vac} \rangle \\ &= \frac{|\tilde{\omega}|}{2} \langle \mathbf{E}_{vac} | \text{Im}\left\{ \frac{e^{i\theta}}{\chi^*} \right\}^{-1} \left[\mathbb{I} - \frac{\text{Asym}(e^{-i\theta}\mathbb{G})}{\text{Im}\{e^{i\theta}/\chi^*\}} + \dots \right] | \mathbf{E}_{vac} \rangle \\ &\leq \frac{|\tilde{\omega}|}{2} \text{Im}\left\{ \frac{e^{i\theta}}{\chi^*} \right\}^{-1} \langle \mathbf{E}_{vac} | \mathbf{E}_{vac} \rangle. \end{aligned} \quad (16)$$

The zeroth-order approximation given in (16) is especially simple to evaluate as it only depends on χ , and will hereafter be referred to as a material bound. A special yet sub-optimal value of θ in (16) recovers prior LDOS bounds based on passivity (SI) [31]. Notably, this zeroth order approximation becomes loose whenever $\text{Im}\{e^{i\theta}/\chi^*\}^{-1} \text{Asym}(e^{-i\theta}\mathbb{G})$ is large as compared to \mathbb{I} ; this is the case for large $|\chi|$ or large design domains (e.g., the half-space) where $\text{Asym}\mathbb{G}$ dominates. Intuitively, terms containing the vacuum Green's function capture physical limitations imposed by multiple scattering, screening, and the finite speed of light, which limit achievable LDOS.

Figure 2 shows upper bounds on the LDOS for both TM and TE sources, obtained by evaluating (15). In the near-field limit of $d \rightarrow 0$, the TM bounds are found to asymptote to a constant while the TE bounds scale $\propto 1/d^2$, in agreement with a detailed asymptotic analysis of the evanescent $k_{\parallel} \rightarrow \infty$ behavior of the integrand in (15) (SI), and matching prior results based on passivity [31]. The constant asymptote observed for TM sources as they approach the device reflects a known artifact of 2d scalar electromagnetism, which precludes non-integrable field singularities at sharp corners [44]. In contrast, the $1/d^2$ scaling of TE sources confirms the known divergence in the energy concentration of a vector dipole in its near field, with the exponent of d tied to the number of spatial dimensions; note that the maximum LDOS for a 3d source grows $\propto 1/d^3$ as $d \rightarrow 0$ (SI).

In the opposite far-field limit of $d \rightarrow \infty$ and for finite Q_{src} , the bounds ultimately tend toward zero, reflecting a kind of space-bandwidth constraint on the ability of structuring to affect far-field emission over a finite bandwidth. One can, however, observe plateaus occurring at intermediate regimes, $\omega d/c \ll Q_{src}$, wherein structuring can efficiently reflect traveling planewaves back onto the dipole position. Achievable enhancements in this regime can be shown to decay $\propto e^{-d/Q_{src}}$, manifesting as plateaus in the various plots of Figure 2b. Only in the strictly single-frequency limit $Q_{src} \rightarrow \infty$ do far-field LDOS contributions tend toward constants, $\rho_0/2$ and ρ_0

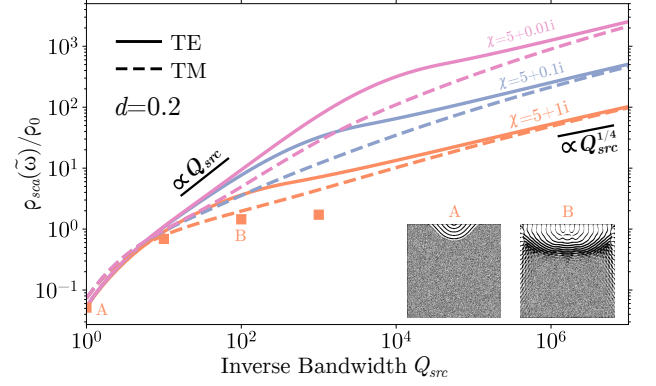


Figure 3. Maximum LDOS enhancement near a halfspace design region as a function of the source bandwidth. Squares are the performance of TM inverse designs over a 10×10 design region for $\chi = 5+1i$, with insets A and B the structures found via TO for $Q_{src} = 1$ and $Q_{src} = 100$ respectively.

for TE and TM sources, respectively, independently of separation. The importance of properly capturing relevant wave interference effects in these far-field regimes becomes evident when analyzing corresponding predictions for material bounds [31], which exhibit drastically inflated $\propto Q_{src}^2$ scaling in this half-space setting (SI).

Asymptotic analysis of (15) supported by Figure 2b reveal that LDOS enhancements saturate to finite values as $|\chi| \rightarrow \infty$ (SI), in contrast to prior bounds which grow indefinitely with increasing material response [31]. This is somewhat surprising given that larger χ implies a larger (potentially infinite) density of states within the material itself; ultimately, multiple scattering and screening effects lead to restrictions on the possible field localization at the source location that cannot be overcome with clever structuring. Similar conclusions have been reached concerning the efficacy of hyperbolic metamaterials [45] at enhancing the LDOS in that particular geometry class. It is also worth noting that the saturation characteristics of the full bounds as a function of d is distinct for the TM and TE polarizations. For TM, reducing d increases the relative advantage of stronger materials; $\rho(\chi \rightarrow \infty) \propto \log(1/d)$ as $d \rightarrow 0$ whereas $\rho(\chi < \infty)$ is finite as $d \rightarrow 0$ (SI). In contrast, for TE the saturation behavior for large $|\chi|$ scales uniformly with d ; decreasing separation does not increase the relative advantage of stronger materials.

With regard to bandwidth scaling, the broad structural freedom afforded by an infinite design domain coupled with the lack of material dissipation allows for creation of resonances with arbitrarily small radiative loss rates, $Q_{mode} \rightarrow \infty$, leading to the same $\propto Q_{src}$ dependence observed in Figure 1. The situation changes in dissipative media where mode lifetimes $Q_{mode} = (\frac{1}{Q_{abs}} + \frac{1}{Q_{rad}})^{-1}$ contain both radiative Q_{rad} and absorptive Q_{abs} contributions, with $Q_{abs} \propto 1/\text{Im}(\chi)$ denoting the proportion

of stored energy dissipated in the medium per unit cycle. Hence, under finite absorption, Q_{abs} sets a bound on the highest achievable mode lifetime, with (11) suggesting a saturating LDOS $\propto Q_{abs}$ as $Q_{src} \rightarrow \infty$.

In contrast, Figure 3 shows that the bounds exhibit a transition from the linear $\propto Q_{src}$ scaling of a wide-bandwidth source coupled to a single resonance toward *diverging* response $\propto Q_{src}^{1/4}$ as $Q_{src} \rightarrow \infty$, with the transition taking place as $Q_{src} \rightarrow Q_{abs}$. Intuitively, in this regime wherein the lifetime of a single resonance is capped, one might expect the optimal design strategy to shift toward exploiting degeneracies. One class of geometry capable of achieving high modal degeneracies are waveguides, e.g., coupled cavities or photonic crystal gratings, which at least in 1d are known to generate van Hove singularities in the density of states [46]. Generally, a spectral singularity of the form $|\omega - \omega_0|^{-\alpha}$, $0 < \alpha < 1$ will yield a Lorentzian-averaged LDOS that scales as

$$\int_{-\infty}^{\infty} \frac{\Delta\omega_{src}/\pi}{(\omega - \omega_0)^2 + \Delta\omega_{src}^2} \frac{1}{|\omega - \omega_0|^\alpha} d\omega \propto \frac{1}{(\Delta\omega_{src})^\alpha} \propto Q_{src}^\alpha. \quad (17)$$

The bounds for the 2d half-space configuration thus suggest the possibility of near-field absorbers supporting quartic “band-edge” dispersions capable of efficiently extracting evanescent fields, resulting in singularities of the form $|\omega - \omega_0|^{-1/4}$ (anomalous quartic “slow” group-velocity dispersions have been studied, for instance, in the context of waveguide solitons[47]). Indeed, TO discovers structures resembling adiabatic gratings (Figure 3 insets) and exhibiting the predicted quartic bandwidth scaling, though eventually saturating due to the finite computational domain (SI).

SUMMARY

We proposed an improved framework for evaluating upper bounds on the LDOS in structured media, and study in detail the effects of source bandwidth, material susceptibility, and device footprint. The bounds provide a strong top-down complement to bottom-up design in at least two ways: First, they are useful in quantifying the optimality of existing “best” structures while diagnosing potential areas of improvement: as seen in narrow bandwidth regimes, existing formulations of inverse design fail to converge upon structures with performance close to the global optimum, often outperformed by traditional ring resonators. Second, they allow studies of fundamental scaling characteristics without prior assumptions on device topology.

For finite bandwidths, the quick saturation of the bounds with design size indicate that a device footprint of a few wavelengths is generally enough to achieve near-optimal performance. The observed saturation with increasing susceptibility has direct implications for mate-

rial choice: a weak material response can be mitigated given sufficient design size and judicious structuring; conversely there are diminishing returns associated with seeking large absolute values of the susceptibility, raising the importance of other concerns such as material loss and dispersion characteristics. The impact of material loss was also evaluated in the context of maximum LDOS above a semi-infinite structure, showing a transition from the intuitive linear $\propto Q_{src}$ scaling expected of single-mode resonant enhancement to a less obvious $\propto Q_{src}^{1/4}$ dependence given absorptive materials, inviting further studies into the associated dispersion engineering mechanisms making such scaling possible. While only results for dielectrics ($\text{Re}(\chi) > 0$) were shown in this paper, the framework can handle metals ($\text{Re}(\chi) < 0$) just as well, yielding broadly similar conclusions.

ACKNOWLEDGMENTS

This work was supported by the National Science Foundation under the Emerging Frontiers in Research and Innovation (EFRI) program, Award No. EFMA-164098 and the Defense Advanced Research Projects Agency (DARPA) under Agreements No. HR00111820046, No. HR00112090011, and No. HR0011047197. The views, opinions and findings expressed herein are those of the authors and should not be interpreted as representing the official views or policies of any institution. R.K.D. gratefully acknowledges financial support from the Princeton Presidential Postdoctoral Research Fellowship and from the National Academies of Science, Engineering, and Medicine Ford Foundation Postdoctoral Fellowship program.

* These two authors contributed equally

† email: pengning@princeton.edu

- [1] L. Novotny and B. Hecht, *Principles of Nano-Optics*, second edition ed. (Cambridge University Press, Cambridge, 2012).
- [2] E. M. Purcell, On the absorption and emission of light by interstellar grains, *The Astrophysical Journal* **158**, 433 (1969).
- [3] G. C. des Francs, P. Bramant, J. Grandidier, A. Bouheliier, J.-C. Weeber, and A. Dereux, Optical gain, spontaneous and stimulated emission of surface plasmon polaritons in confined plasmonic waveguide, *Optics Express* **18**, 16327 (2010).
- [4] W. L. Barnes, S. A. R. Horsley, and W. L. Vos, Classical antennas, quantum emitters, and densities of optical states, *Journal of Optics* **22**, 073501 (2020).
- [5] J. Michon, M. Benzaouia, W. Yao, O. D. Miller, and S. G. Johnson, Limits to surface-enhanced Raman scattering near arbitrary-shape scatterers, *Optics Express* **27**, 35189 (2019).

- [6] S. V. Gaponenko, D. V. Guzatov, and N. D. Strekal, Strong Selective Anti-Stokes Raman Scattering Enhancement in Plasmonics Using Photon Density of States Engineering, *The Journal of Physical Chemistry C* **125**, 27654 (2021).
- [7] P. Wang and R. Menon, Optimization of generalized dielectric nanostructures for enhanced light trapping in thin-film photovoltaics via boosting the local density of optical states, *Optics Express* **22**, A99 (2014).
- [8] J. C. Cuevas and F. J. García-Vidal, Radiative Heat Transfer, *ACS Photonics* **5**, 3896 (2018).
- [9] Z. Lin, X. Liang, M. Lončar, S. G. Johnson, and A. W. Rodriguez, Cavity-enhanced second-harmonic generation via nonlinear-overlap optimization, *Optica* **3**, 233 (2016).
- [10] C. Roques-Carmes, N. Rivera, A. Ghorashi, S. E. Kooi, Y. Yang, Z. Lin, J. Beroz, A. Massuda, J. Sloan, N. Romeo, Y. Yu, J. D. Joannopoulos, I. Kaminer, S. G. Johnson, and M. Soljačić, A framework for scintillation in nanophotonics, *Science* **375**, eabm9293 (2022).
- [11] K. J. Vahala, Optical microcavities, *Nature* **424**, 839 (2003).
- [12] D. K. Armani, T. J. Kippenberg, S. M. Spillane, and K. J. Vahala, Ultra-high-Q toroid microcavity on a chip, *Nature* **421**, 925 (2003).
- [13] J. J. Baumberg, J. Aizpurua, M. H. Mikkelsen, and D. R. Smith, Extreme nanophotonics from ultrathin metallic gaps, *Nature Materials* **18**, 668 (2019).
- [14] R. Chikkaraddy, B. de Nijs, F. Benz, S. J. Barrow, O. A. Scherman, E. Rosta, A. Demetriadou, P. Fox, O. Hess, and J. J. Baumberg, Single-molecule strong coupling at room temperature in plasmonic nanocavities, *Nature* **535**, 127 (2016).
- [15] A. Kinkhabwala, Z. Yu, S. Fan, Y. Avlasevich, K. Müllen, and W. E. Moerner, Large single-molecule fluorescence enhancements produced by a bowtie nanoantenna, *Nature Photonics* **3**, 654 (2009).
- [16] J. D. Joannopoulos, J. G. Steven, J. N. Winn, and R. D. Meade, *Photonic Crystals: Molding the Flow of Light*, 2nd ed. (Princeton University Press, Princeton, 2008).
- [17] A. Karamlou, M. E. Trusheim, and D. Englund, Metal-dielectric antennas for efficient photon collection from diamond color centers, *Optics Express* **26**, 3341 (2018).
- [18] A. Pick, B. Zhen, O. D. Miller, C. W. Hsu, F. Hernandez, A. W. Rodriguez, M. Soljačić, and S. G. Johnson, General theory of spontaneous emission near exceptional points, *Optics Express* **25**, 12325 (2017).
- [19] Z. Lin, A. Pick, M. Lončar, and A. W. Rodriguez, Enhanced spontaneous emission at third-order Dirac exceptional points in inverse-designed photonic crystals, *Physical Review Letters* **117**, 107402 (2016).
- [20] S. J. Dewhurst, D. Granados, D. J. P. Ellis, A. J. Bennett, R. B. Patel, I. Farrer, D. Anderson, G. A. C. Jones, D. A. Ritchie, and A. J. Shields, Slow-light-enhanced single quantum dot emission in a unidirectional photonic crystal waveguide, *Applied Physics Letters* **96**, 031109 (2010).
- [21] F. Wang, R. E. Christiansen, Y. Yu, J. Mørk, and O. Sigmund, Maximizing the quality factor to mode volume ratio for ultra-small photonic crystal cavities, *Applied Physics Letters* **113**, 241101 (2018).
- [22] M. Albrechtsen, B. V. Lahijani, R. E. Christiansen, V. T. H. Nguyen, L. N. Casses, S. E. Hansen, N. Stenger, O. Sigmund, H. Jansen, J. Mørk, *et al.*, Nanometer-scale photon confinement inside dielectrics, arXiv:2108.01681 (2021), arXiv:2108.01681.
- [23] S. Molesky, Z. Lin, A. Y. Piggott, W. Jin, J. Vučković, and A. W. Rodriguez, Inverse design in nanophotonics, *Nature Photonics* **12**, 659 (2018).
- [24] P. Chao, B. Strekha, R. Kuate Defo, S. Molesky, and A. W. Rodriguez, Physical limits in electromagnetism, *Nature Reviews Physics* **4**, 543 (2022).
- [25] S. M. Barnett and R. Loudon, Sum Rule for Modified Spontaneous Emission Rates, *Physical Review Letters* **77**, 2444 (1996).
- [26] S. Scheel, Sum rule for local densities of states in absorbing dielectrics, *Physical Review A* **78**, 013841 (2008).
- [27] S. Sanders and A. Manjavacas, Analysis of the Limits of the Local Density of Photonic States near Nanostructures, *ACS Photonics* **5**, 2437 (2018).
- [28] A. Raman, W. Shin, and S. Fan, Upper Bound on the Modal Material Loss Rate in Plasmonic and Metamaterial Systems, *Physical Review Letters* **110**, 183901 (2013).
- [29] Q. Zhao, L. Zhang, and O. D. Miller, Minimum Dielectric-Resonator Mode Volumes (2020), arXiv:2008.13241 [physics].
- [30] O. D. Miller, A. G. Polimeridis, M. T. H. Reid, C. W. Hsu, B. G. DeLacy, J. D. Joannopoulos, M. Soljačić, and S. G. Johnson, Fundamental limits to optical response in absorptive systems, *Optics Express* **24**, 3329 (2016).
- [31] H. Shim, L. Fan, S. G. Johnson, and O. D. Miller, Fundamental Limits to Near-Field Optical Response over Any Bandwidth, *Physical Review X* **9**, 011043 (2019).
- [32] X. Liang and S. G. Johnson, Formulation for scalable optimization of microcavities via the frequency-averaged local density of states, *Optics Express* **21**, 30812 (2013).
- [33] J. D. Jackson, *Classical Electrodynamics*, 3rd ed. (Wiley, New York, 1999).
- [34] W. R. Hindmarsh and D. ter Haar, *Atomic Spectra: The Commonwealth and International Library: Selected Readings in Physics* (Elsevier Science, Kent, 2014).
- [35] R. E. Christiansen and O. Sigmund, Inverse design in photonics by topology optimization: Tutorial, *JOSA B* **38**, 496 (2021).
- [36] G. Angeris, J. Vučković, and S. Boyd, Heuristic methods and performance bounds for photonic design, *Optics Express* **29**, 2827 (2021).
- [37] S. P. Boyd and L. Vandenberghe, *Convex Optimization* (Cambridge University Press, Cambridge, UK ; New York, 2004).
- [38] E. a. J. Marcatili, Bends in Optical Dielectric Guides, *Bell System Technical Journal* **48**, 2103 (1969).
- [39] B. V. Budaev and D. B. Bogy, On the electromagnetic field singularities near the vertex of a dielectric wedge, *Radio Science* **42**, 10.1029/2006RS003578 (2007).
- [40] S. Chakravarthi, P. Chao, C. Pederson, S. Molesky, A. Ivanov, K. Hestroffer, F. Hatami, A. W. Rodriguez, and K.-M. C. Fu, Inverse-designed photon extractors for optically addressable defect qubits, *Optica* **7**, 1805 (2020).
- [41] R. A. Wambold, Z. Yu, Y. Xiao, B. Bachman, G. Jaffe, S. Kolkowitz, J. T. Choy, M. A. Eriksson, R. J. Hamers, and M. A. Kats, Adjoint-optimized nanoscale light extractor for nitrogen-vacancy centers in diamond, *Nanophotonics* **10**, 393 (2021).
- [42] L. Li, E. H. Chen, J. Zheng, S. L. Mouradian, F. Dolde, T. Schröder, S. Karaveli, M. L. Markham, D. J. Twitchen, and D. Englund, Efficient Photon Collection

- from a Nitrogen Vacancy Center in a Circular Bullseye Grating, *Nano Letters* **15**, 1493 (2015).
- [43] A. Rodriguez, M. Ibanescu, J. D. Joannopoulos, and S. G. Johnson, Disorder-immune confinement of light in photonic-crystal cavities, *Optics Letters* **30**, 3192 (2005).
 - [44] J. Andersen and V. Solodukhov, Field behavior near a dielectric wedge, *IEEE Transactions on Antennas and Propagation* **26**, 598 (1978).
 - [45] O. D. Miller, S. G. Johnson, and A. W. Rodriguez, Effectiveness of thin films in lieu of hyperbolic metamaterials in the near field, *Physical Review Letters* **112**, 157402 (2014).
 - [46] M. Ibanescu, E. J. Reed, and J. D. Joannopoulos, Enhanced Photonic Band-Gap Confinement via Van Hove Saddle Point Singularities, *Physical Review Letters* **96**, 033904 (2006).
 - [47] A. Blanco-Redondo, C. M. de Sterke, J. E. Sipe, T. F. Krauss, B. J. Eggleton, and C. Husko, Pure-quartic solitons, *Nature Communications* **7**, 10427 (2016).

Maximum Electromagnetic Local Density of States via Material Structuring: Supplementary Information

Pengning Chao*, Rodrick Kuate Defo*, Sean Molesky, Alejandro Rodriguez

October 4, 2022

Contents

1	Computational Details	3
2	Dependence of bounds on number of subregion constraints	3
3	Ring resonator LDOS enhancement	4
4	Bandwidth saturation of finite size LDOS bounds	4
5	Differences in notation in supplementary information compared to the main text	5
6	Derivation of power conservation constraints via complex Poynting's theorem	5
6.1	Complex Poynting's theorem for time harmonic fields and complex ω	5
6.2	Generalized energy conservation constraints	6
7	Lagrangian duality given global constraints	8
8	Spectral analysis of Green's function	9
9	Spectral Analysis of $\text{Asym}(p\mathbb{U})$	10
9.1	Lossless dielectrics	11
10	Global constraint bounds for 2D TM dipole near a half-space	12
10.1	TM Green's function and dipole field	12
10.2	Simplification of (S24)	12
10.3	Evaluation of $\text{Asym}(p\mathbb{U}^{TM})^{-1} \mathbf{E}_v^{TM}\rangle$	13
10.4	TE Green's function and dipole field	16
11	Asymptotic analysis	17
11.1	TM bandwidth scaling	17
11.1.1	Traveling wave contribution	17
11.1.2	Evanescant wave contribution	19
11.2	TM material Scaling	20
11.3	TM separation scaling	20

11.3.1	Finite χ	21
11.3.2	Material independent bounds	21
11.4	TE separation scaling	21
11.4.1	3D separation scaling	22
12	Comparison to passivity bounds	22
12.1	Bandwidth scaling of the passivity bounds	23

1 Computational Details

Inverse design in this work was performed using the ceviche Maxwell FDFD solver [1] combined with the method of moving asymptotes algorithm as implemented in the non-linear optimization package NLOPT [2].

Finite size LDOS bounds were computed using an in-house FDFD code to represent the Green's function and the electric fields over the design domain. The dual function is optimized with an in-house implementation of BFGS; for details on the computation of the dual gradient see [3].

2 Dependence of bounds on number of subregion constraints

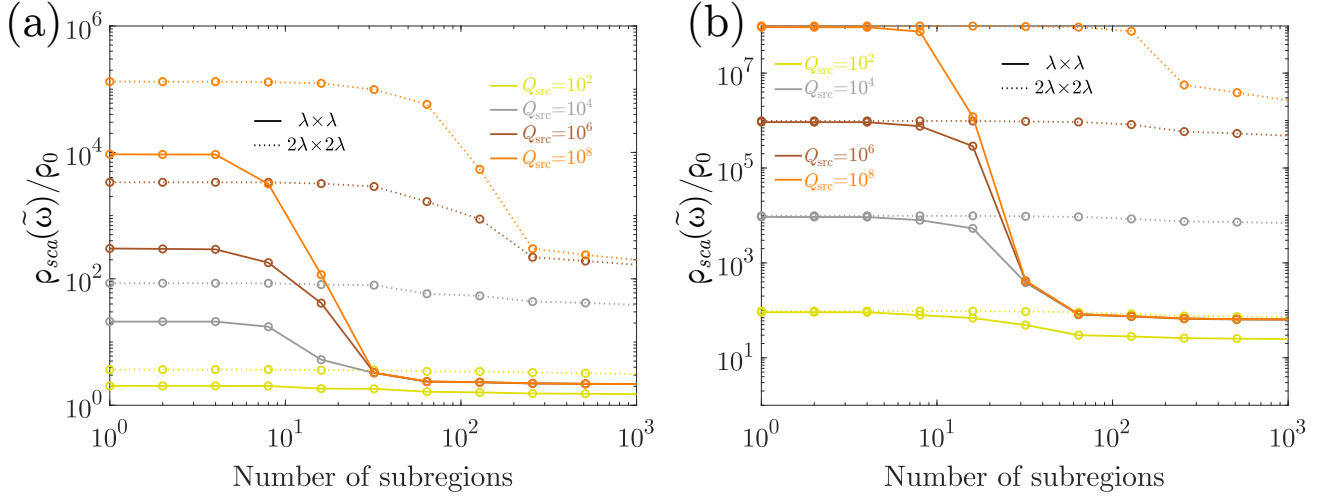


Figure S1: Plot showing the computed LDOS dual bounds as a function of the number of subregion constraints used. The subplots (a) and (b) correspond to the exterior dipole and interior dipole geometries shown in Fig. 1 of the main text. Solid lines are for system size $L = 1$ and dotted lines are for system size $L = 2$.

Fig. S1 shows how the bounds depend on the number of subregion constraints used. Generally there is a rapid transition of many orders of magnitude when the number of subregions reaches a critical value before convergence of the bounds. For larger Q_{src} the transition is steeper, indicating the importance of subregion constraints for capturing the effects of radiative loss. For larger system size L , the transition is shallower: as stated in the main text, in the limit of large L global constraints alone are sufficient to achieve tight bounds.

3 Ring resonator LDOS enhancement

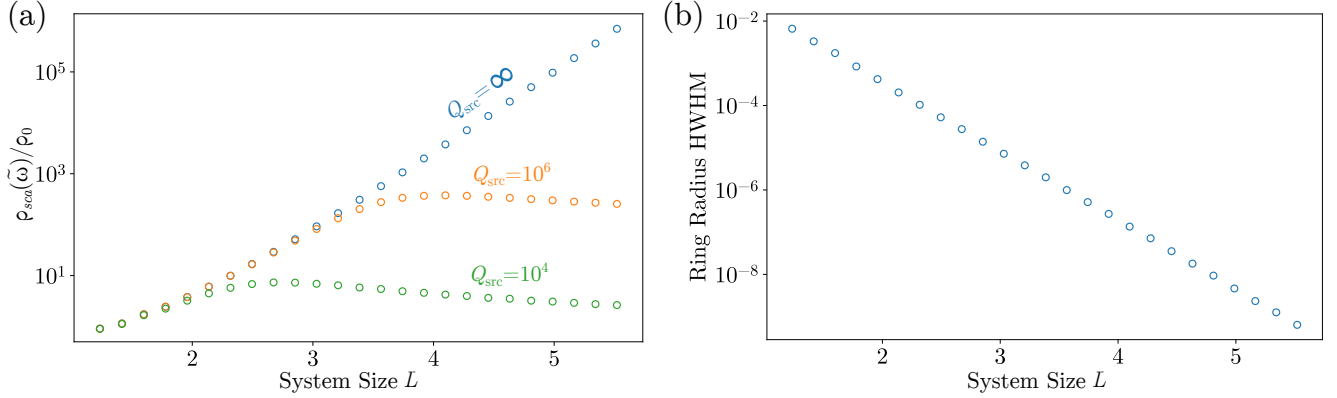


Figure S2: (a) LDOS enhancement of ring resonators with a fixed ring width of 0.2 and TM dipole source separated 0.2 away from the ring. The system size L is 2 times the outer radius of the rings. (b) At $Q_{src} \rightarrow \infty$, the change in the ring radius Δr such that the LDOS enhancement drops by a half.

In the main text we presented a specific ring resonator design with a ring width of 0.2 that outperformed topology optimization from multiple random initializations. Here are extra data on the performance of ring resonators as a function of size for various Q_{src} . In the single frequency limit, we see the exponential scaling of LDOS enhancement as a function of ring size; for finite Q_{src} there is a point where larger rings have higher Q_{mode} but do not lead to larger bandwidth-averaged LDOS. For the $Q_{src} = 10^6$ design shown in the main text the outer ring diameter is approximately 4.1; Fig. S2b indicates that we require around 8 significant figures of accuracy on the ring size to fall within 50% of the maximum performance.

4 Bandwidth saturation of finite size LDOS bounds

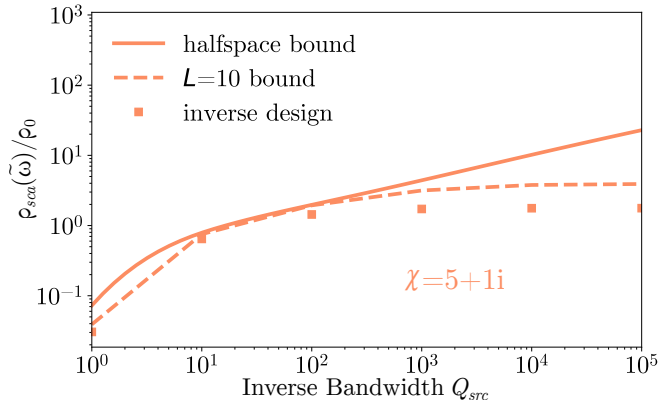


Figure S3: LDOS bounds as a function of Q_{src} for $\chi = 5 + 1i$.

In Fig. 3 of the main text, the inverse designs are performed over a finite design domain of size 10 by 10, and the LDOS enhancement saturates with increasing Q_{src} . Fig. S3 shows that this

saturation is also present we you compute the bounds for the finite design domain; continued $Q_{src}^{1/4}$ scaling is seen just for the semi-infinite halfspace bounds.

5 Differences in notation in supplementary information compared to the main text

In the following sections, some quantities and variables use a different notation than what is written in the main text. This is predominantly for conciseness in writing down long derivations. For convenience a complete list of the differences in notation is listed here; each individual notation deviation will also be noted at its first occurrence in the SI.

- The vacuum field \mathbf{E}_{vac} in main text is referred to as \mathbf{E}_v in the SI.
- Use of k_x and k_y instead of k_{\parallel} and k_{\perp} for half-space bounds, with the \hat{x} direction set as parallel to the half-space surface and \hat{y} direction perpendicular to it.
- the complex parameters $R_{1,2}$ and $r_{1,2}$ in the main text are replaced with R_{\pm} and r_{\pm} in the SI, where the \pm subscripts have more background context within the derivation.
- With dimensionless units $c = 1$, $\tilde{k} = \tilde{\omega}/c$ will often be used in place $\tilde{\omega}$ in the context of spatial Fourier integrals.

6 Derivation of power conservation constraints via complex Poynting's theorem

Here we present a derivation of the complex scattering constraints used via the complex Poynting's Theorem. For alternative derivations see early work [...].

6.1 Complex Poynting's theorem for time harmonic fields and complex ω

In prior literature the complex Poynting's Theorem for time harmonic fields is presented given a real angular frequency ω . The generalization to a complex ω is straightforward and written explicitly here for clarity. All fields have (complex) harmonic time dependence $e^{-i\omega t}$, with the harmonic time Maxwell's equations

$$\nabla \cdot \mathbf{D} = \rho_f \tag{S1a}$$

$$\nabla \cdot \mathbf{B} = 0 \tag{S1b}$$

$$\nabla \times \mathbf{E} = i\omega \mathbf{B} \tag{S1c}$$

$$\nabla \times \mathbf{H} = \mathbf{J}_f - i\omega \mathbf{D} \tag{S1d}$$

and linear constitutive relations $\mathbf{D}(\mathbf{r}) = \epsilon_0 \bar{\epsilon}_r(\mathbf{r}) \mathbf{E}(\mathbf{r})$ and $\mathbf{B}(\mathbf{r}) = \mu_0 \bar{\mu}_r(\mathbf{r}) \mathbf{H}(\mathbf{r})$, with $\bar{\epsilon}(\mathbf{r})$ and $\bar{\mu}(\mathbf{r})$ being tensor fields to allow for anisotropy.

Define the complex Poynting vector

$$\mathbf{S} = \mathbf{E} \times \mathbf{H}^* \tag{S2}$$

Taking its divergence yields

$$\nabla \cdot \mathbf{E} \times \mathbf{H}^* = \mathbf{H}^* \cdot \nabla \times \mathbf{E} - \mathbf{E} \cdot \nabla \times \mathbf{H}^* \quad (\text{S3})$$

Now applying Maxwell's equations gives the differential form of the complex Poynting's theorem

$$\begin{aligned} \nabla \cdot \mathbf{E} \times \mathbf{H}^* &= i\omega \mathbf{H}^* \times \mathbf{B} - i\omega^* \mathbf{E} \cdot \mathbf{D}^* - \mathbf{E} \cdot \mathbf{J}^* \\ &= i\omega \mathbf{H}^* \cdot \bar{\boldsymbol{\mu}} \cdot \mathbf{H} - i\omega^* \mathbf{E} \cdot \bar{\boldsymbol{\epsilon}}^* \cdot \mathbf{E}^* - \mathbf{E} \cdot \mathbf{J}^* \end{aligned} \quad (\text{S4})$$

The corresponding integral form is

$$\int_{\partial V} d\sigma \cdot (\mathbf{E} \times \mathbf{H}^*) = i\omega \int_V \mathbf{H}^* \cdot \bar{\boldsymbol{\mu}} \cdot \mathbf{H} dV - i\omega^* \int_V \mathbf{E} \cdot \bar{\boldsymbol{\epsilon}}^* \cdot \mathbf{E}^* dV - \int_V \mathbf{E} \cdot \mathbf{J}^* dV \quad (\text{S5})$$

in the case where ω is real we have

$$\int_{\partial V} d\sigma \cdot (\mathbf{E} \times \mathbf{H}^*) = i\omega \int_V (\mathbf{H}^* \cdot \bar{\boldsymbol{\mu}} \cdot \mathbf{H} - \mathbf{E} \cdot \bar{\boldsymbol{\epsilon}}^* \cdot \mathbf{E}^*) dV - \int_V \mathbf{E} \cdot \mathbf{J}^* dV \quad (\text{S6})$$

which is a more familiar form.

6.2 Generalized energy conservation constraints

To arrive at the generalized energy conservation constraints, we start with a scattering theory framework in which an initial free current source \mathbf{J}_v produces the fields $\mathbf{E}_v, \mathbf{H}_v$ in vacuum. These initial fields interact with a scatterer, producing polarization currents \mathbf{J}_s within the scatterer that generate scattered fields $\mathbf{E}_s, \mathbf{H}_s$. For simplicity, we assume that the scatterer is non-magnetic, i.e., $\bar{\boldsymbol{\mu}} = \mu_0$, and that the electric permittivity is local but may be anisotropic: $\bar{\boldsymbol{\epsilon}}_r = \epsilon_0(\mathbb{I} + \mathbb{I}_s \bar{\boldsymbol{\chi}} \mathbb{I}_s)$. The net result is a total field $\mathbf{E}_t = \mathbf{E}_v + \mathbf{E}_s, \mathbf{H}_t = \mathbf{H}_v + \mathbf{H}_s$. The complex Poynting theorem then applies in three settings: to the free current and initial fields $(\mathbf{J}_v, \mathbf{E}_v, \mathbf{H}_v)$ in vacuum, to the polarization current and scattered fields $(\mathbf{J}_s, \mathbf{E}_s, \mathbf{H}_s)$ in vacuum, and to the free current and total fields $(\mathbf{J}_v, \mathbf{E}_t, \mathbf{H}_t)$.

We consider as our region of interest some subset V_k of the design region. For $(\mathbf{J}_v, \mathbf{E}_v, \mathbf{H}_v)$ in vacuum we have

$$\int_{\partial V_k} d\sigma \cdot (\mathbf{E}_v \times \mathbf{H}_v) = i\omega\mu_0 \int_{V_k} \mathbf{H}_v^* \cdot \mathbf{H}_v dV - i\omega^*\epsilon_0 \int_{V_k} \mathbf{E}_v \cdot \mathbf{E}_v^* dV. \quad (\text{S7})$$

For $(\mathbf{J}_s, \mathbf{E}_s, \mathbf{H}_s)$ in vacuum we have

$$\int_{\partial V_k} d\sigma \cdot (\mathbf{E}_s \times \mathbf{H}_s) = i\omega\mu_0 \int_{V_k} \mathbf{H}_s^* \cdot \mathbf{H}_s dV - i\omega^*\epsilon_0 \int_{V_k} \mathbf{E}_s \cdot \mathbf{E}_s^* dV - \int_{V_k} \mathbf{E}_s \cdot \mathbf{J}_s^* dV. \quad (\text{S8})$$

For $(\mathbf{J}_v, \mathbf{E}_t, \mathbf{H}_t)$ with the scatterer we have (noting that the free current is situated outside of the design region)

$$\begin{aligned} &\int_{\partial V_k} d\sigma \cdot ((\mathbf{E}_v + \mathbf{E}_s) \times (\mathbf{H}_v + \mathbf{H}_s)) \\ &= i\omega\mu_0 \int_{V_k} (\mathbf{H}_v^* + \mathbf{H}_s^*) \cdot (\mathbf{H}_v + \mathbf{H}_s) dV - i\omega^*\epsilon_0 \int_{V_k} (\mathbf{E}_v + \mathbf{E}_s) \cdot (\mathbb{I} + \mathbb{I}_s \bar{\boldsymbol{\chi}}^* \mathbb{I}_s) \cdot (\mathbf{E}_v^* + \mathbf{E}_s^*) dV. \end{aligned} \quad (\text{S9})$$

Subtracting (S7) and (S8) from (S9) gives

$$\begin{aligned}
& \int_{\partial V_k} d\sigma \cdot (\mathbf{E}_v \times \mathbf{H}_s + \mathbf{E}_s \times \mathbf{H}_v) \\
&= i\omega\mu_0 \int_{V_k} (\mathbf{H}_v^* \cdot \mathbf{H}_s + \mathbf{H}_s^* \cdot \mathbf{H}_v) dV \\
&\quad - i\omega^*\epsilon_0 \int_{V_k} [\mathbf{E}_v \cdot \mathbb{I}_s \bar{\chi}^* \mathbb{I}_s \cdot \mathbf{E}_v^* + \mathbf{E}_s \cdot \mathbb{I}_s \bar{\chi}^* \mathbb{I}_s \cdot \mathbf{E}_s^* + \mathbf{E}_v \cdot (\mathbb{I} + \mathbb{I}_s \bar{\chi}^* \mathbb{I}_s) \cdot \mathbf{E}_s^* + \mathbf{E}_s \cdot (\mathbb{I} + \mathbb{I}_s \bar{\chi}^* \mathbb{I}_s) \cdot \mathbf{E}_v^*] dV \\
&\quad + \int_{V_k} \mathbf{E}_s \cdot \mathbf{J}_s^* dV.
\end{aligned} \tag{S10}$$

To further simplify this expression, we investigate the cross term

$$\mathbf{H}_v^* \cdot \mathbf{H}_s = \frac{1}{\mu_0^2 |\omega|^2} (\nabla \times \mathbf{E}_s) \cdot (\nabla \times \mathbf{E}_v^*) = \frac{1}{\mu_0^2 |\omega|^2} \nabla \cdot (\mathbf{E}_s \times \nabla \times \mathbf{E}_v^*) + \frac{1}{\mu_0^2 |\omega|^2} \mathbf{E}_s \cdot \nabla \times \nabla \times \mathbf{E}_v^*$$

where we have used the identity

$$(\nabla \times \mathbf{A}) \cdot \mathbf{B} = \nabla \cdot (\mathbf{A} \times \mathbf{B}) + \mathbf{A} \cdot (\nabla \times \mathbf{B}).$$

Now \mathbf{E}_v satisfies the vector wave equation

$$\begin{aligned}
& \nabla \times \nabla \times \mathbf{E}_v - \frac{\omega^2}{c^2} \mathbf{E}_v = 0 \\
& \Rightarrow \nabla \times \nabla \times \mathbf{E}_v^* = \frac{\omega^{*2}}{c^2} \mathbf{E}_v^*
\end{aligned}$$

over a source-free vacuum region, leading to

$$\mathbf{H}_v^* \cdot \mathbf{H}_s = \frac{1}{\mu_0^2 |\omega|^2} \nabla \cdot (\mathbf{E}_s \times \nabla \times \mathbf{E}_v^*) + \frac{\omega^*}{\mu_0^2 c^2 \omega} \mathbf{E}_s \cdot \mathbf{E}_v^*,$$

$$\begin{aligned}
i\omega\mu_0 \int_{V_k} \mathbf{H}_v^* \cdot \mathbf{H}_s dV &= \frac{i}{\mu\omega^*} \int_{\partial V_k} d\sigma \cdot (\mathbf{E}_s \times \nabla \times \mathbf{E}_v^*) + i\omega^*\epsilon_0 \int_{V_k} \mathbf{E}_s \cdot \mathbf{E}_v^* dV \\
&= \int_{\partial V_k} d\sigma \cdot (\mathbf{E}_s \times \mathbf{H}_v^*) + i\omega^*\epsilon_0 \int_{V_k} \mathbf{E}_s \cdot \mathbf{E}_v^* dV.
\end{aligned}$$

Thus we have the useful relation

$$i\omega\mu_0 \int_{V_k} \mathbf{H}_v^* \cdot \mathbf{H}_s dV - \int_{\partial V_k} d\sigma \cdot (\mathbf{E}_s \times \mathbf{H}_v^*) - i\omega^*\epsilon_0 \int_{V_k} \mathbf{E}_s \cdot (\mathbb{I} + \mathbb{I}_s \bar{\chi}^* \mathbb{I}_s) \cdot \mathbf{E}_v^* dV = -i\omega^*\epsilon_0 \int_{V_k} \mathbf{E}_s \cdot \mathbb{I}_s \bar{\chi}^* \mathbb{I}_s \cdot \mathbf{E}_v^* dV. \tag{S11}$$

Similarly the other cross terms satisfy the relation

$$\begin{aligned}
& i\omega\mu_0 \int_{V_k} \mathbf{H}_v^* \cdot \mathbf{H}_s dV - \int_{\partial V_k} d\sigma \cdot (\mathbf{E}_s \times \mathbf{H}_v^*) - i\omega^*\epsilon_0 \int_{V_k} \mathbf{E}_s \cdot (\mathbb{I} + \mathbb{I}_s \bar{\chi}^* \mathbb{I}_s) \cdot \mathbf{E}_v^* dV \\
&= -i\omega^*\epsilon_0 \int_{V_k} \mathbf{E}_s \cdot \mathbb{I}_s \bar{\chi}^* \mathbb{I}_s \cdot \mathbf{E}_v^* dV + \int_{V_k} \mathbf{E}_v \cdot \mathbf{J}_s^* dV
\end{aligned} \tag{S12}$$

where the additional $\int_{V_k} \mathbf{E}_v \cdot \mathbf{J}_s^* dV$ comes from \mathbf{E}_s satisfying a vector wave equation with the polarization currents as source:

$$\nabla \times \nabla \times \mathbf{E}_s - \frac{\omega^2}{c^2} \mathbf{E}_s = i\omega\mu_0 \mathbf{J}_s.$$

Substituting these cross-term relations into the expression and taking the complex conjugate gives

$$\int_{V_k} \mathbf{E}_v^* \cdot \mathbf{J}_s dV = -i\omega\epsilon_0 \int_{V_k} \mathbf{E}_t^* \cdot \mathbb{I}_s \bar{\chi} \mathbb{I}_s \cdot \mathbf{E}_t dV - \int_{V_k} \mathbf{E}_s^* \cdot \mathbf{J}_s dV. \quad (\text{S13})$$

At this point, we can replace the polarization current \mathbf{J}_s , scattered electric field E_s , and total electric field E_t with the polarization density \mathbf{P} via the following relations

$$\mathbf{J}_s = -i\omega \mathbf{P} \quad \mathbf{P} = \epsilon_0 \bar{\chi} \mathbb{I}_s \cdot \mathbf{E}_t \quad \mathbf{E}_s = \frac{1}{\epsilon_0} \mathbb{G} \cdot \mathbf{P} \quad (\text{S14})$$

to finally obtain

$$\int_{V_k} \mathbf{E}_v \cdot \left(\frac{\mathbf{P}}{\epsilon_0} \right) dV = \int_{V_k} \left(\frac{\mathbf{P}}{\epsilon_0} \right)^* \cdot \left(\frac{1}{\chi^*} - \mathbb{G}^* \right) \cdot \left(\frac{\mathbf{P}}{\epsilon_0} \right) dV. \quad (\text{S15})$$

7 Lagrangian duality given global constraints

In this section we detail how the dual problem for the two global power conservation constraints is equivalent to the dual problem for a single constraint with an additional parameter in the form of a complex phase rotation.

We are interested in placing dual bounds on the power extracted from a dipole source given global conservation of power:

$$\text{maximize} \quad \rho_{sca} = -\frac{1}{2} \text{Im}\{\tilde{\omega} \langle \mathbf{E}_i^* | \mathbf{P} \rangle\} \quad (\text{S16a})$$

$$\text{such that} \quad \text{Re} \langle \mathbf{E}_v | \mathbf{P} \rangle - \langle \mathbf{P} | \text{Sym} \mathbb{U} | \mathbf{P} \rangle = 0 \quad (\text{S16b})$$

$$\text{Im} \langle \mathbf{E}_v | \mathbf{P} \rangle - \langle \mathbf{P} | \text{Asym} \mathbb{U} | \mathbf{P} \rangle = 0. \quad (\text{S16c})$$

The Lagrangian for this constrained optimization problem is

$$\begin{aligned} \mathcal{L}(\mathbf{P}, \alpha_{Re}, \alpha_{Im}) &= -\frac{1}{2} \text{Im}\{\tilde{\omega} \langle \mathbf{E}_i^* | \mathbf{P} \rangle\} + \alpha_{Re} [\text{Re} \langle \mathbf{E}_v | \mathbf{P} \rangle - \langle \mathbf{P} | \text{Sym} \mathbb{U} | \mathbf{P} \rangle] + \alpha_{Im} [\text{Im} \langle \mathbf{E}_v | \mathbf{P} \rangle - \langle \mathbf{P} | \text{Asym} \mathbb{U} | \mathbf{P} \rangle] \\ &= -\frac{1}{2} \text{Im}\{\tilde{\omega} \langle \mathbf{E}_i^* | \mathbf{P} \rangle\} + \left(\frac{\alpha_{Re}}{2} + \frac{\alpha_{Im}}{2i} \right) \langle \mathbf{E}_v | \mathbf{P} \rangle + \left(\frac{\alpha_{Re}}{2} - \frac{\alpha_{Im}}{2i} \right) \langle \mathbf{P} | \mathbf{E}_v \rangle \\ &\quad + \langle \mathbf{P} | \left[\left(\frac{\alpha_{Re}}{2} + \frac{\alpha_{Im}}{2i} \right) \mathbb{U} + \left(\frac{\alpha_{Re}}{2} - \frac{\alpha_{Im}}{2i} \right) \mathbb{U}^\dagger \right] | \mathbf{P} \rangle, \end{aligned}$$

With the corresponding dual function

$$\mathcal{D}(\alpha_{Re}, \alpha_{Im}) = \max_{\mathbf{P}} \mathcal{L}(\mathbf{P}, \alpha_{Re}, \alpha_{Im}). \quad (\text{S17})$$

Now define $\alpha \equiv \sqrt{\alpha_{Re}^2 + \alpha_{Im}^2}$ and a complex phase rotation $p \equiv e^{i\theta} = (\alpha_{Im} + i\alpha_{Re})/\alpha$ the Lagrangian can be re-written as

$$\begin{aligned} \mathcal{L}(\mathbf{P}, \alpha; \theta) &= -\frac{1}{2} \text{Im}\{\tilde{\omega} \langle \mathbf{E}_i^* | \mathbf{P} \rangle\} + \alpha \left(\frac{e^{i\theta} \langle \mathbf{E}_i^* | \mathbf{P} \rangle - e^{-i\theta} \langle \mathbf{P} | \mathbf{E}_i^* \rangle}{2i} - \langle \mathbf{P} | \frac{e^{i\theta} \mathbb{U} - e^{-i\theta} \mathbb{U}^\dagger}{2i} | \mathbf{P} \rangle \right) \\ &= -\frac{1}{2} \text{Im}\{\tilde{\omega} \langle \mathbf{E}_i^* | \mathbf{P} \rangle\} + \alpha [\text{Im}(p \langle \mathbf{E}_i^* | \mathbf{P} \rangle) - \langle \mathbf{P} | \text{Asym}(p\mathbb{U}) | \mathbf{P} \rangle] \end{aligned} \quad (\text{S18})$$

which is exactly the Lagrangian of the single constraint optimization

$$\text{maximize } \rho_{sca} = -\frac{1}{2} \text{Im}\{\tilde{\omega} \langle \mathbf{E}_i^* | \mathbf{P} \rangle\} \quad (\text{S19a})$$

$$\text{such that } \text{Im}(p \langle \mathbf{E}_v | \mathbf{P} \rangle) - \langle \mathbf{P} | \text{Asym}(p\mathbb{U}) | \mathbf{P} \rangle = 0 \quad (\text{S19b})$$

with corresponding dual function

$$\mathcal{D}(\alpha; \theta) = \max_{\mathbf{P}} \mathcal{L}(\mathbf{P}, \alpha; \theta). \quad (\text{S20})$$

Now it is clear that $(e^{i\theta}, \alpha)$ is just an alternate parametrization of the multiplier space of $(\alpha_{Re}, \alpha_{Im})$, hence the tightest dual bound is

$$\min_{\alpha_{Re}, \alpha_{Im}} \mathcal{D}(\alpha_{Re}, \alpha_{Im}) = \min_{\theta} \min_{\alpha} \mathcal{D}(\alpha; \theta). \quad (\text{S21})$$

We can now derive an expression for $\min_{\alpha} \mathcal{D}(\alpha; \theta)$ for fixed phase rotation θ . First, note that the Lagrangian $\mathcal{L}(\mathbf{P}, \alpha; \theta)$ only has a finite maximum when $\text{Asym}(p\mathbb{U}) \succ 0$. See the following section for a spectral analysis of $\text{Asym}(p\mathbb{U})$ ascertaining the existence and range of complex phase rotation p such that $\text{Asym}(p\mathbb{U}) \succ 0$. We evaluate (S20) by calculating the stationary point of \mathcal{L} with respect to $|\mathbf{P}\rangle$:

$$\frac{\partial \mathcal{L}}{\partial \langle \mathbf{P} |} = 0 \quad \Rightarrow \quad |\mathbf{P}\rangle = -\frac{i\tilde{\omega}^*}{4\alpha} \text{Asym}(p\mathbb{U})^{-1} |\mathbf{E}_v^*\rangle + \frac{i}{2} p^* \text{Asym}(p\mathbb{U})^{-1} |\mathbf{E}_v\rangle. \quad (\text{S22})$$

This stationary point maximizes \mathcal{L} when $\text{Asym}(p\mathbb{U}) \succ 0$. Given this positive definite condition, the primal problem (S19) is also a convex problem with a non-empty feasible set, so strong duality holds [cite]. Thus to solve for the optimal $\bar{\alpha}$ that minimizes $\mathcal{D}(\alpha; \theta)$, we substitute (S22) into (S19b) and obtain

$$\bar{\alpha} = \sqrt{\frac{|\tilde{\omega}|^2}{4|p|^2} \frac{\langle \mathbf{E}_v^* | \text{Asym}(p\mathbb{U})^{-1} | \mathbf{E}_v^* \rangle}{\langle \mathbf{E}_v | \text{Asym}(p\mathbb{U})^{-1} | \mathbf{E}_v \rangle}}. \quad (\text{S23})$$

Now (S22) and (S23) can be simultaneously substituted back into (S20) to get the bound

$$\begin{aligned} \rho_{sca} \leq \min_{\alpha} \mathcal{D}(\alpha; \theta) &= \frac{|\tilde{\omega}|}{4} \sqrt{\langle \mathbf{E}_v^* | \text{Asym}(p\mathbb{U})^{-1} | \mathbf{E}_v^* \rangle \langle \mathbf{E}_v | \text{Asym}(p\mathbb{U})^{-1} | \mathbf{E}_v \rangle} \\ &\quad - \frac{1}{4} \text{Re} \left\{ p^* \tilde{\omega} \langle \mathbf{E}_v^* | \text{Asym}(p\mathbb{U})^{-1} | \mathbf{E}_v \rangle \right\} \end{aligned} \quad (\text{S24})$$

as seen in the main text.

8 Spectral analysis of Green's function

Notation: in this and future sections of the supplementary info we will sometimes use the spatial wavevector $\tilde{k} = \tilde{\omega}/c = \tilde{\omega}$; in the main text only $\tilde{\omega}$ is used to reduce the number of different variables shown and to take advantage of the dimensionless units $c = 1$.

Starting from the planewave expansion of \mathbb{G} as given by [6] (multiplied by \tilde{k}^2 following our convention)

$$\mathbb{G} = \frac{1}{(2\pi)^3} \iiint d^3\mathbf{k} e^{i\mathbf{k} \cdot (\mathbf{r} - \mathbf{r}')} \frac{\mathbb{I}\tilde{k}^2 - \mathbf{k} \otimes \mathbf{k}}{k^2 - \tilde{k}^2}, \quad (\text{S25})$$

we have

$$\text{Asym}\mathbb{G} = \frac{1}{(2\pi)^3} \iiint d^3\mathbf{k} e^{i\mathbf{k}\cdot(\mathbf{r}-\mathbf{r}')} \left\{ \text{Im} \left(\frac{\tilde{k}^2}{k^2 - \tilde{k}^2} \right) \mathbb{I} - \text{Im} \left(\frac{k^2}{k^2 - \tilde{k}^2} \right) \hat{\mathbf{k}} \otimes \hat{\mathbf{k}} \right\}. \quad (\text{S26})$$

Now $\tilde{k}^2 = \tilde{k}_r^2 - \tilde{k}_i^2 + 2i\tilde{k}_r\tilde{k}_i$; for notational convenience define $A_r \equiv \text{Re}\{\tilde{k}^2\} = \tilde{k}_r^2 - \tilde{k}_i^2$ and $A_i = \text{Im}\{\tilde{k}^2\} = 2\tilde{k}_r\tilde{k}_i$. Taking the imaginary part, we get

$$\text{Asym}\mathbb{G} = \frac{1}{(2\pi)^3} \iiint d^3\mathbf{k} e^{i\mathbf{k}\cdot(\mathbf{r}-\mathbf{r}')} \left\{ \frac{A_i k^2}{(k^2 - A_r)^2 + A_i^2} \mathbb{I} - \frac{A_i k^2}{(k^2 - A_r)^2 + A_i^2} \hat{\mathbf{k}} \otimes \hat{\mathbf{k}} \right\}. \quad (\text{S27})$$

It is apparent now that the eigenwaves of $\text{Asym}\mathbb{G}$ have the form $\hat{\mathbf{e}} e^{i\mathbf{k}\cdot\mathbf{r}}$, where $\hat{\mathbf{e}}$ is an eigenvector of the 3×3 matrix in parentheses. Under a triad that includes $\hat{\mathbf{k}}$, the 3×3 matrix is diagonal, and we see the longitudinal eigenwaves $\hat{\mathbf{k}} e^{i\mathbf{k}\cdot\mathbf{r}}$ have eigenvalue 0. The transverse eigenwaves have eigenvalues

$$\rho_t(k) = \frac{A_i k^2}{(k^2 - A_r)^2 + A_i^2} = \frac{2\tilde{k}_r\tilde{k}_i k^2}{(k^2 - \tilde{k}_r^2 + \tilde{k}_i^2)^2 + (2\tilde{k}_r\tilde{k}_i)^2} \geq 0. \quad (\text{S28})$$

Some observations about the scaling of these eigenvalues that are relevant for later discussion:

- $\text{Asym}\mathbb{G}$ is positive semi-definite. The null-space always includes the longitudinal waves (which are irrelevant to the TM case). For single frequencies $\tilde{k}_i = 0$ the null-space includes all evanescent waves; for finite bandwidth $\tilde{k}_i > 0$ the null-space only contains extremely fast oscillations / extreme evanescent waves in the limit $|k| \rightarrow \infty$.
- Some idea of the scaling of $\text{Asym}\mathbb{G}^{-1}$ can be seen through the inverse of the transverse eigenvalues $1/\rho_t = \frac{1}{A_i} k^2 + \left(\frac{A_r^2}{A_i} + A_i\right) \frac{1}{k^2} - 2\frac{A_r}{A_i}$, which for $k \geq \tilde{k}_r$ has a minimum around $k = |\tilde{k}|$ before scaling $\sim k^2$ as $k \rightarrow \infty$.

9 Spectral Analysis of $\text{Asym}(p\mathbb{U})$

We have $\text{Asym}(p\mathbb{U}) = \text{Asym}(\chi^{-1\dagger}p) + \text{Asym}(p^*\mathbb{G})$. $\text{Asym}(\chi^{-1\dagger}p)$ contributes a constant to all eigenvalues; we focus our attention on the second term $\text{Asym}(p^*\mathbb{G})$. Similar to the analysis in the previous subsection, we have

$$\text{Asym}\mathbb{G} = \frac{1}{(2\pi)^3} \iiint d^3\mathbf{k} e^{i\mathbf{k}\cdot(\mathbf{r}-\mathbf{r}')} \left\{ \text{Im} \left(\frac{p^* \tilde{k}^2}{k^2 - \tilde{k}^2} \right) \mathbb{I} - \text{Im} \left(\frac{p^* k^2}{k^2 - \tilde{k}^2} \right) \hat{\mathbf{k}} \otimes \hat{\mathbf{k}} \right\}. \quad (\text{S29})$$

The longitudinal and transverse eigenvalues of $\text{Asym}(p^*\mathbb{G})$ come out to be

$$\begin{aligned} \rho_{\mathbb{G},l}(p) &= p_i, \\ \rho_{\mathbb{G},t}(p) &= \frac{p_r k^2 A_i + p_i [-A_r(k^2 - A_r) + A_i^2]}{(k^2 - A_r)^2 + A_i^2}. \end{aligned}$$

The eigenvalues of $\text{Asym}(p\mathbb{U})$ are

$$\rho_{\mathbb{U},l} = \frac{\chi_i}{\chi_r^2 + \chi_i^2} p_r + \left(1 + \frac{\chi_r}{\chi_r^2 + \chi_i^2}\right) p_i, \quad (\text{S30})$$

$$\rho_{\mathbb{U},t} = \frac{p_r \chi_i + p_i \chi_r}{\chi_r^2 + \chi_i^2} + \frac{p_r k^2 A_i + p_i [-A_r(k^2 - A_r) + A_i^2]}{(k^2 - A_r)^2 + A_i^2}. \quad (\text{S31})$$

In order for the dual bound (S24) to be valid we need $\text{Asym}(p\mathbb{U})$ to be positive definite, i.e., $\rho_{\mathbb{U}} > 0$.

9.1 Lossless dielectrics

For lossless dielectrics we have $\chi_i = 0$, $\chi_r > 0$. The PD condition $\rho_{\mathbb{U},t} > 0$ then leads to $p_i > 0$. Setting $p_r = 1$, we require

$$\rho_{\mathbb{U},t} = \frac{1}{\chi_r} p_i + \frac{k^2 A_i + p_i [-A_r(k^2 - A_r) + A_i^2]}{(k^2 - A_r)^2 + A_i^2} > 0. \quad (\text{S32})$$

Defining for convenience $u \equiv k^2$, the problem is then finding

$$\min_{u \geq 0} f(u) = \frac{(A_i - p_i A_r)u + p_i(A_r^2 + A_i^2)}{(u - A_r)^2 + A_i^2}. \quad (\text{S33})$$

It is clear that $f(0) = p_i > 0$ and $\lim_{u \rightarrow \infty} f(u) = 0$. In the special case $p_i = A_i/A_r$, the only critical point is $u^* = A_r$ which is a maximum, so $\min f(u) = 0$ and $\rho_{\mathbb{U},t} = \frac{1}{\chi_r} p_i > 0$. When $p_i \neq A_i/A_r$ the critical points are (assuming $A_i \ll A_r$)

$$u^{*\pm} \approx \frac{p_i A_r^2 \pm \sqrt{1 + p_i^2} A_i A_r}{p_i A_r - A_i}. \quad (\text{S34})$$

If $p_i < A_i/A_r$ then $u^{*+} < 0$ and irrelevant, while u^{*-} is a maximum, so $\min f(u) = 0$. If $p_i > A_i/A_r$, then u^{*+} is the minimum, with

$$\min f(u) = f(u^{*+}) \approx \frac{-\sqrt{1 + p_i^2} A_r A_i}{\left[\frac{(1 + \sqrt{1 + p_i^2}) A_r A_i}{p_i A_r - A_i} \right]^2 + A_i^2} < 0. \quad (\text{S35})$$

Thus for lossless dielectrics, $\text{Asym}(p\mathbb{U})$ is PD given $p_r = 1$ and $0 < p_i \leq A_i/A_r$. For specific values of χ_r , larger rotation angles with $p_i > A_i/A_r$ is possible. By how much? Set

$$p_i = c \cdot \frac{A_i}{A_r}; \quad (\text{S36})$$

now, assume that $p_i \ll 1$ in the limit $A_i \rightarrow 0$ for vanishing bandwidth, this assumption can be checked for consistency at the end. This yields

$$\min f(u) \approx -\frac{(c-1)^2}{4} \frac{A_i}{A_r}. \quad (\text{S37})$$

Then

$$\rho_{\mathbb{U},t} > 0 \Rightarrow \frac{p_i}{\chi_r} > \frac{(c-1)^2}{4} \frac{A_i}{A_r} \Rightarrow c^2 - \left(\frac{4}{\chi_r} + 2 \right) c + 1 < 0. \quad (\text{S38})$$

Conclude that

$$c < 1 + 2 \left[\frac{1}{\chi_r} + \sqrt{\frac{1}{\chi_r^2} + \frac{1}{\chi_r}} \right], \quad (\text{S39})$$

so c_{\max} is a monotonic function of χ_r and not dependent on the bandwidth, $p_{i,\max} \propto A_i \ll 1$ in the limit $A_i \rightarrow 0$.

10 Global constraint bounds for 2D TM dipole near a half-space

In this section we evaluate (S24) explicitly for the case of 2D TM dipole source $\mathbf{J}(x', y') = \delta(x')\delta(y' + d)$ a distance d away from a half-space design region $V = \{(x, y) | y > 0\}$.

Notation: in the main text the \parallel and \perp symbols were used to indicate directions parallel and perpendicular to the surface of the half-space design region, respectively. In this section we use explicit Cartesian coordinates with x being \parallel and y being \perp .

10.1 TM Green's function and dipole field

Following [6], the 2D TM Green's function is

$$\mathbb{G}^{TM}(\rho, \rho') = \tilde{k}^2 \frac{i}{4\pi} \begin{cases} \int_{-\infty}^{\infty} dk_x \frac{\hat{z}\hat{z}}{k_y} e^{ik_x(x-x')} e^{ik_y(y-y')} & y > y' \\ \int_{-\infty}^{\infty} dk_x \frac{\hat{z}\hat{z}}{k_y} e^{ik_x(x-x')} e^{-ik_y(y-y')} & y < y' \end{cases} \quad (\text{S40})$$

where $\tilde{k} = \tilde{k}_r + i\tilde{k}_i$ is complex for finite bandwidths, $k_y = \sqrt{\tilde{k}^2 - k_x^2}$ always taking the root with positive imaginary part.

The dipole source $\mathbf{J}(x', y') = \delta(x')\delta(y' + d)$ produces a vacuum electric field within the $y > 0$ design region

$$\mathbf{E}_v^{TM}(x, y) = \int_{-\infty}^{\infty} \frac{e^{ik_x x}}{\sqrt{2\pi}} \mathbf{E}_{v,k_x}^{TM}(y) dk_x, \quad (\text{S41a})$$

$$\mathbf{E}_{v,k_x}^{TM}(y) = -\frac{\tilde{k}}{2\sqrt{2\pi}} \frac{1}{k_y} e^{ik_y y} e^{ik_y d}. \quad (\text{S41b})$$

The single frequency vacuum dipole radiation is

$$\rho_0^{TM} = \frac{\text{Re}\{\tilde{k}\}}{8} = \frac{\pi}{4\lambda_0}. \quad (\text{S42})$$

The composite $\text{Asym}(p\mathbb{U}^{TM})$ integral operator is

$$\text{Asym}(p\mathbb{U}^{TM})(x, y, x', y') = \int_{-\infty}^{\infty} dk_x \frac{e^{ik_x x}}{\sqrt{2\pi}} \text{Asym}(p\mathbb{U}^{TM})_{k_x}(y, y') \frac{e^{-ik_x x'}}{\sqrt{2\pi}} \quad (\text{S43a})$$

with

$$\text{Asym}(p\mathbb{U}^{TM})_{k_x}(y, y') = \text{Im}\{p/\chi^*\} \delta(y - y') + \frac{1}{2} \text{Re}\left\{p^* \frac{\tilde{k}^2}{k_y} e^{ik_y|y-y'|}\right\}. \quad (\text{S43b})$$

10.2 Simplification of (S24)

For the half-space design region, (S24) may be simplified by observing that $\langle \mathbf{E}_v^{TM} | \text{Asym}(p\mathbb{U}^{TM})^{-1} | \mathbf{E}_v^{TM} \rangle = \langle \mathbf{E}_v^{TM*} | \text{Asym}(p\mathbb{U}^{TM})^{-1} | \mathbf{E}_v^{TM*} \rangle$. We have

$$\langle \mathbf{E}_v^{TM} | \text{Asym}(p\mathbb{U}^{TM})^{-1} | \mathbf{E}_v^{TM} \rangle = \frac{|\tilde{k}|^2}{8\pi} \int_{-\infty}^{\infty} dk_x \frac{e^{-2k_y d}}{|k_y|^2} \iint_0^{\infty} e^{-ik_y^* y} \text{Asym}(p\mathbb{U}^{TM})_{k_x}^{-1}(y, y') e^{ik_y y} dy' dy \quad (\text{S44})$$

where we have made multiple use of the Fourier completeness relation $\frac{1}{2\pi} \int_{-\infty}^{\infty} e^{i(k_x - k'_x)x} dx = \delta(k_x - k'_x)$. Now,

$$\begin{aligned} \mathbf{E}_v^{TM*}(x, y) &= -\frac{\tilde{k}^*}{2\sqrt{2\pi}} \int_{-\infty}^{\infty} \frac{e^{-ik_x x}}{\sqrt{2\pi}} \frac{1}{k_y^*} e^{-ik_y^* y} e^{-ik_y^* d} dk_x \\ &= -\frac{\tilde{k}^*}{2\sqrt{2\pi}} \int_{-\infty}^{\infty} \frac{e^{ik_x x}}{\sqrt{2\pi}} \frac{1}{k_y^*} e^{-ik_y^* y} e^{-ik_y^* d} dk_x \quad kx \rightarrow -kx \end{aligned} \quad (\text{S45})$$

where in the second line we have made use of the fact that $k_y = \sqrt{\tilde{k}^2 - k_x^2}$ is invariant to the sign of k_x . This gives

$$\langle \mathbf{E}_v^{TM} | \text{Asym}(p\mathbb{U}^{TM})^{-1} | \mathbf{E}_v^{TM} \rangle = \frac{|\tilde{k}|^2}{8\pi} \int_{-\infty}^{\infty} dk_x \frac{e^{-2k_y d}}{|k_y|^2} \iint_0^{\infty} e^{ik_y y} \text{Asym}(p\mathbb{U}^{TM})_{k_x}^{-1}(y, y') e^{-ik_y^* y} dy' dy. \quad (\text{S46})$$

Now from (S43b) we see that $\text{Asym}(p\mathbb{U}^{TM})_{k_x}(y, y')$ is invariant under exchange of the y, y' dummy integration variables. Since (S44) and (S46) are related by the exchange of y, y' , conclude that

$$\langle \mathbf{E}_v^{TM} | \text{Asym}(p\mathbb{U}^{TM})^{-1} | \mathbf{E}_v^{TM} \rangle = \langle \mathbf{E}_v^{TM*} | \text{Asym}(p\mathbb{U}^{TM})^{-1} | \mathbf{E}_v^{TM*} \rangle. \quad (\text{S47})$$

This allows us to simplify (S24) to

$$\rho_{sca}^{TM} \leq \frac{|\tilde{\omega}|}{4} \langle \mathbf{E}_v^{TM} | \text{Asym}(p\mathbb{U}^{TM})^{-1} | \mathbf{E}_v^{TM} \rangle - \frac{1}{4} \text{Re} \left\{ p^* \tilde{\omega} \langle \mathbf{E}_v^{TM*} | \text{Asym}(p\mathbb{U})^{-1} | \mathbf{E}_v^{TM} \rangle \right\}. \quad (\text{S48})$$

For certain asymptotic and approximation analyses, we will also make use of (S47) and the Cauchy-Schwartz inequality to relax the second term in (S48), yielding

$$\rho_{sca}^{TM} \leq \frac{|\tilde{\omega}|}{2} \langle \mathbf{E}_v^{TM} | \text{Asym}(p\mathbb{U}^{TM})^{-1} | \mathbf{E}_v^{TM} \rangle \quad (\text{S49})$$

10.3 Evaluation of $\text{Asym}(p\mathbb{U}^{TM})^{-1} | \mathbf{E}_v^{TM} \rangle$

The core calculation in (S48) is the evaluation of

$$\text{Asym}(p\mathbb{U}^{TM})^{-1} | \mathbf{E}_v^{TM} \rangle = -\frac{\tilde{k}}{2\sqrt{2\pi}} \int_{-\infty}^{\infty} dk_x \frac{e^{ik_x x}}{\sqrt{2\pi}} \frac{e^{ik_y d}}{k_y} \int_0^{\infty} \text{Asym}(p\mathbb{U}^{TM})_{k_x}^{-1}(y, y') e^{ik_y y'} dy'. \quad (\text{S50})$$

Defining

$$f(y) = \int_0^{\infty} \text{Asym}(p\mathbb{U}^{TM})_{k_x}^{-1}(y, y') e^{ik_y y'} dy', \quad (\text{S51})$$

we have

$$\int_0^{\infty} \text{Asym}(p\mathbb{U}^{TM})_{k_x}(y, y') f(y') dy' = e^{ik_y y}. \quad (\text{S52})$$

The action of $\text{Asym}(p\mathbb{U})_{k_x}$ is a convolution over y ; this suggests that the Laplace transform $\mathcal{L}\{h(t)\}(s) = \int_0^{\infty} h(t) e^{-st} dt$ may be used to solve (S52). We now take the Laplace transform of both sides of (S52), defining $F(s) \equiv \mathcal{L}\{f(y)\}$ and the auxiliary variable $B \equiv p^* \frac{\tilde{k}^2}{k_y}$. The LHS gives

$$\begin{aligned} \text{Im} \left\{ \frac{p}{\chi^*} \right\} F(s) &+ \frac{B_r + iB_i}{4} \mathcal{L} \left\{ \int_0^y e^{-(k_{yi} - ik_{yr})(y-y')} f(y') dy' \right\} + \frac{B_r - iB_i}{4} \mathcal{L} \left\{ \int_0^y e^{-(k_{yi} + ik_{yr})(y-y')} f(y') du' \right\} \\ &+ \frac{B_r + iB_i}{4} \mathcal{L} \left\{ \int_y^{\infty} e^{(k_{yi} - ik_{yr})(y-y')} f(y') dy' \right\} + \frac{B_r - iB_i}{4} \mathcal{L} \left\{ \int_y^{\infty} e^{(k_{yi} + ik_{yr})(y-y')} f(y') dy' \right\}. \end{aligned}$$

The RHS is simply

$$\mathcal{L}\left\{e^{(-k_{yi}+ik_{yr})y}\right\} = \frac{1}{s + (k_{yi} - ik_{yr})}.$$

Evaluating the LHS, the Laplace transform of a convolution gives

$$\mathcal{L}\left\{\int_0^y e^{-a(y-y')} f(y') dy'\right\} = \frac{F(s)}{s + a}. \quad (\text{S53})$$

The transform of the other type of integral can be evaluated explicitly to a simple form:

$$\begin{aligned} \mathcal{L}\left\{\int_y^\infty e^{a(y-y')} f(y') dy'\right\} &= \int_0^\infty e^{-sy} \int_y^\infty e^{a(y-y')} f(y') dy' dy \\ &= \int_0^\infty e^{-ay'} f(y') \left(\int_0^{y'} e^{-(s-a)y} dy\right) dy' \quad \text{exchange order of integration} \\ &= \int_0^\infty f(y') e^{-ay'} \frac{1}{a-s} \left(e^{(a-s)y'} - 1\right) dy' \\ &= \frac{1}{a-s} \left(\int_0^\infty f(y') e^{-sy'} dy' - \int_0^\infty f(y') e^{-ay'} dy'\right) \\ &= \frac{1}{a-s} (F(s) - F(a)). \end{aligned} \quad (\text{S54})$$

Thus $F(s)$ satisfies

$$\begin{aligned} \frac{1}{s + (k_{yi} - ik_{yr})} &= \frac{p_i}{\chi} F(s) + \frac{Br + iB_i}{4} \frac{F(s)}{s + (k_{yi} - ik_{yr})} \\ &\quad + \frac{Br - iB_i}{4} \frac{F(s)}{s + (k_{yi} + ik_{yr})} \\ &\quad + \frac{Br + iB_i}{4} \frac{1}{(k_{yi} - ik_{yr}) - s} \left[F(s) - F(k_{yi} - ik_{yr})\right] \\ &\quad + \frac{Br - iB_i}{4} \frac{1}{(k_{yi} + ik_{yr}) - s} \left[F(s) - F(k_{yi} + ik_{yr})\right]. \end{aligned} \quad (\text{S55})$$

Solving this will give us an explicit form of $F(s)$ dependent on two free parameters $F(k_{yi} - ik_{yr})$ and $F(k_{yi} + ik_{yr})$. This seemingly gives, instead of a single solution $f(y)$, a whole family of solutions. However, as we shall see, only one member of this family belongs to $L^2[0, \infty)$, decaying as $y \rightarrow \infty$. The other members of this family grow exponentially as $y \rightarrow \infty$ which violates the requirements of Fubini's theorem [4] needed to justify the order of integration exchange used in (S54), and are not true solutions to (S52).

Solving for $F(s)$ yields

$$F(s) = \frac{F_{num}(s)}{F_{denom}(s)} \quad (\text{S56a})$$

where the numerator is

$$\begin{aligned} F_{num}(s) &= [s - (k_{yi} - ik_{yr})][s^2 - (k_{yi} + ik_{yr})^2] - \frac{Br + iB_i}{4} \gamma_- [s + (k_{yi} - ik_{yr})][s^2 - (k_{yi} + ik_{yr})^2] \\ &\quad - \frac{Br - iB_i}{4} \gamma_+ [s + (k_{yi} + ik_{yr})][s^2 - (k_{yi} - ik_{yr})^2] \end{aligned} \quad (\text{S56b})$$

and the denominator is

$$F_{denom}(s) = \text{Im}\left\{\frac{p}{\chi^*}\right\} s^4 - \left[2 \text{Im}\left\{\frac{p}{\chi^*}\right\} (k_{yi}^2 - k_{yr}^2) + (B_r k_{yi} + B_i k_{yr})\right] s^2 + \text{Im}\left\{\frac{p}{\chi^*}\right\} |k_y|^4 + (B_r k_{yi} - B_i k_{yr}) |k_y|^2, \quad (\text{S56c})$$

where for notational convenience, we have defined $\gamma_{\pm} \equiv F(k_{yi} \pm i k_{yr})$.

The roots r of $F_{denom}(s)$ are then the poles of $F(s)$:

$$(+, -)r_+ = (+, -) \left\{ (k_{yi}^2 - k_{yr}^2) + \frac{1}{2 \text{Im}\{p/\chi^*\}} \left[(B_r k_{yi} + B_i k_{yr}) + \sqrt{\Delta} \right] \right\}^{1/2}, \quad (\text{S57a})$$

$$(+, -)r_- = (+, -) \left\{ (k_{yi}^2 - k_{yr}^2) + \frac{1}{2 \text{Im}\{p/\chi^*\}} \left[(B_r k_{yi} + B_i k_{yr}) - \sqrt{\Delta} \right] \right\}^{1/2}, \quad (\text{S57b})$$

$$\Delta = (B_r k_{yi} + B_i k_{yr})^2 + 8 \text{Im}\left\{\frac{p}{\chi^*}\right\} \left(B_i k_{yr} k_{yi}^2 - B_r k_{yr}^2 k_{yi} - \text{Im}\left\{\frac{p}{\chi^*}\right\} k_{yr}^2 k_{yi}^2 \right), \quad (\text{S57c})$$

$$F_{denom}(s) = \text{Im}\left\{\frac{p}{\chi^*}\right\} (s - r_+)(s + r_+)(s - r_-)(s + r_-). \quad (\text{S57d})$$

We see that the poles come in two pairs $\pm r_+$ and $\pm r_-$. In general, one each from $(+, -)r_+$ and $(+, -)r_-$ will have a positive real part and its opposite sign counterpart will have a negative real part; we take r_+ and r_- to be the poles with positive real parts (in the main text these are r_1 and r_2 respectively). The inverse Laplace transform is

$$f(y) = \mathcal{L}^{-1}\left\{F(s)\right\} = \frac{1}{2\pi i} \int_{T-i\infty}^{T+i\infty} F(s) e^{sy} ds \quad (\text{S58})$$

where $T \in \mathbb{R}$ is greater than the real parts of all the poles of $F(s)$. Since $y > 0$, we can deform the line integration and complete the contour in the $\text{Re}\{s\} < 0$ half plane upon which the contour completion part decays to 0; thus the inverse Laplace transform picks out the residue of $F(s)e^{sy}$. It is clear then that the contribution to the residue from r_+ and r_- leads to functions with exponential growth as $y \rightarrow \infty$ whereas the contribution from $-r_+$ and $-r_-$ lead to functions with exponential decay as $y \rightarrow \infty$. To recover $f(y) \in L^2[0, \infty)$ we need to select free parameters γ_{\pm} such that the residue for r_+ and r_- are 0. This leads to the following linear system of equations from which we solve for γ_{\pm} :

$$\begin{aligned} & [r_+ - (k_{yi} - i k_{yr})][r_+^2 - (k_{yi} + i k_{yr})^2] \\ &= \frac{B_r + i B_i}{4} [r_+ + (k_{yi} - i k_{yr})][r_+^2 - (k_{yi} + i k_{yr})^2] \gamma_- + \frac{B_r - i B_i}{4} [r_+ + (k_{yi} + i k_{yr})][r_+^2 - (k_{yi} - i k_{yr})^2] \gamma_+, \end{aligned} \quad (\text{S59a})$$

$$\begin{aligned} & [r_- - (k_{yi} - i k_{yr})][r_-^2 - (k_{yi} + i k_{yr})^2] \\ &= \frac{B_r + i B_i}{4} [r_- + (k_{yi} - i k_{yr})][r_-^2 - (k_{yi} + i k_{yr})^2] \gamma_- + \frac{B_r - i B_i}{4} [r_- + (k_{yi} + i k_{yr})][r_-^2 - (k_{yi} - i k_{yr})^2] \gamma_+. \end{aligned} \quad (\text{S59b})$$

$f(y)$ then takes on the form

$$f(y) = R_+ e^{-r_+ y} + R_- e^{-r_- y} \quad (\text{S60})$$

with the coefficients of the exponentials (R_1 and R_2 in the main text) given by

$$R_{\pm} = \frac{1}{\mp 2 \operatorname{Im}\{p/\chi^*\} r_{\pm} \cdot (r_+^2 - r_-^2)} \left\{ [-r_{\pm} - (k_{yi} - ik_{yr})][r_{\pm}^2 - (k_{yi} + ik_{yr})^2] \right. \\ \left. - \frac{B_r + iB_i}{4} [-r_{\pm} + (k_{yi} - ik_{yr})][r_{\pm}^2 - (k_{yi} + ik_{yr})^2] \gamma_- \right. \\ \left. - \frac{B_r - iB_i}{4} [-r_{\pm} + (k_{yi} + ik_{yr})][r_{\pm}^2 - (k_{yi} - ik_{yr})^2] \gamma_+ \right\}. \quad (\text{S61})$$

(S60) can now be substituted back into (S50) and (S48) to get an analytical integral expression for the LDOS enhancement bound near a half-space:

$$\rho_{sca} \leq \frac{1}{16\pi} \int_0^{\infty} \operatorname{Re} \left\{ -\frac{\tilde{k}^3 p e^{2ik_y d}}{k_y^2} \left(\frac{R_+}{r_+ - ik_y} + \frac{R_-}{r_- - ik_y} \right) + \frac{|\tilde{k}|^3 e^{-2k_y d}}{|k_y|^2} \left(\frac{R_+}{r_+ + ik_y^*} + \frac{R_-}{r_- + ik_y^*} \right) \right\} \quad (\text{S62})$$

10.4 TE Green's function and dipole field

The 2D TE Green's function is

$$\mathbb{G}^{TE}(x, y, x', y') = -\hat{y}\hat{y}\delta(x - x')\delta(y - y') + \tilde{k}^2 \frac{i}{4\pi} \begin{cases} \int_{-\infty}^{\infty} dk_x \frac{\hat{h}(k_y)\hat{h}(k_y)}{k_y} e^{ik_x(x-x')} e^{ik_y(y-y')} & y > y' \\ \int_{-\infty}^{\infty} dk_x \frac{\hat{h}(-k_y)\hat{h}(-k_y)}{k_y} e^{ik_x(x-x')} e^{-ik_y(y-y')} & y < y' \end{cases} \quad (\text{S63})$$

with the unit vectors \hat{h} given by

$$\hat{h}(k_y) = -\frac{k_y}{\tilde{k}}\hat{x} + \frac{k_x}{\tilde{k}}\hat{y} \quad \hat{h}(-k_y) = \frac{k_y}{\tilde{k}}\hat{x} + \frac{k_x}{\tilde{k}}\hat{y}. \quad (\text{S64})$$

A dipole source of the form $\mathbf{J}^y(x', y') = \hat{y}\delta(x')\delta(y' + d)$ produces a vacuum field

$$\mathbf{E}_v^{TEy}(x, y) = \int_{-\infty}^{\infty} \frac{e^{ik_x x}}{\sqrt{2\pi}} \mathbf{E}_{v,k_x}^{TEy}(y) dk_x, \quad (\text{S65a})$$

$$\mathbf{E}_{v,k_x}^{TEy}(y) = -\frac{\sqrt{2\pi}}{4\pi\tilde{k}} \cdot e^{ik_y d} e^{ik_y y} \cdot \left(-k_x \hat{x} + \frac{k_x^2}{k_y} \hat{y} \right). \quad (\text{S65b})$$

The vacuum dipole radiation is

$$\rho_0^{TEy} = \frac{\operatorname{Re}\{\tilde{k}\}}{16} = \frac{\pi}{8\lambda_0}. \quad (\text{S66})$$

The composite $\operatorname{Asym}(p\mathbb{U}^{TE})$ integral operator is

$$\operatorname{Asym}(p\mathbb{U}^{TE}) = \int_{-\infty}^{\infty} dk_x \frac{e^{ik_x(x-x')}}{2\pi} \left\{ \operatorname{Im}\left\{ \frac{p}{\chi^*} \right\} \delta(y - y') (\hat{x}\hat{x} + \hat{y}\hat{y}) + \delta(y - y') p_i \hat{y}\hat{y} + \right. \\ \left. \frac{1}{2} \operatorname{Re}\left\{ p^* k_y e^{ik_y|y-y'|} \right\} \hat{x}\hat{x} + \frac{1}{2} \operatorname{Re}\left\{ p^* (k_x^2/k_y) e^{ik_y|y-y'|} \right\} \hat{y}\hat{y} - \frac{1}{2} \operatorname{sgn}(y - y') \operatorname{Im}\left\{ p^* k_x e^{ik_y|y-y'|} \right\} (\hat{x}\hat{y} + \hat{y}\hat{x}) \right\}. \quad (\text{S67})$$

The corresponding global constraint bound for a TE dipole source near a half-space can be derived following an analogous procedure to that of a TM dipole source, though the expressions involved are tedious and was done in practice using Mathematica. For conciseness, the expressions are not reproduced here.

11 Asymptotic analysis

Based on the results from the prior Section, we can do asymptotic analysis to understand the observed scaling of the half-space bounds with regards to bandwidth, material, and separation.

11.1 TM bandwidth scaling

To understand the scaling of the LDOS bounds with bandwidth, it is illuminating to consider the contributions from the traveling waves and evanescent waves separately. Here traveling waves and evanescent waves refer to different k_x in the planewave decomposition of the dipole field: traveling waves have $|k_x| < \tilde{k}_r$ and a predominantly real k_y , propagating for long distances with decay rate proportional to the bandwidth \tilde{k}_i ; evanescent waves have $|k_x| > \tilde{k}_r$ and a predominantly imaginary k_y , rapidly decaying along the y direction with decay rate strongly dependent on $|k_x|$.

11.1.1 Traveling wave contribution

We show that in the limit of zero bandwidth / single frequency, the contribution from just the traveling waves to the LDOS limits tends toward a finite constant. The following analysis is for TM fields but an analogous result can be obtained for TE fields.

We take the material susceptibility $|\chi| \rightarrow \infty$ and phase rotation $p = 1$ so the results are material-independent and $\text{Asym}(p\mathbb{U}^{TM}) = \text{Asym}\mathbb{G}^{TM}$:

$$\begin{aligned} \text{Asym}\mathbb{G}^{TM}(x, y; x', y') &= \int_{-\infty}^{\infty} \frac{e^{ik_x(x-x')}}{2\pi} \text{Asym}\mathbb{G}_{k_x}^{TM}(y, y') dk_x, \\ \text{Asym}\mathbb{G}_{k_x}^{TM}(y, y') &= \frac{1}{2} \text{Re} \left\{ \frac{\tilde{k}^2}{k_y} e^{ik_y|y-y'|} \right\}. \end{aligned}$$

In the limit of zero bandwidth / single frequency, $\tilde{k} \in \mathbb{R}$. Then for $|k_x| > \tilde{k}$, k_y is purely imaginary and $\text{Asym}\mathbb{G}_{k_x}^{TM} = 0$, leading to

$$\begin{aligned} \text{Asym}\mathbb{G}^{TM} &= \int_{-\tilde{k}}^{\tilde{k}} dk_x \frac{e^{ik_x(x-x')}}{2\pi} \frac{\tilde{k}^2}{k_y} \cos k_y(y - y') \\ &= \int_{-\tilde{k}}^{\tilde{k}} dk_x \frac{e^{ik_x(x-x')}}{2\pi} \frac{\tilde{k}^2}{k_y} [\cos(k_y y) \cos(k_y y') + \sin(k_y y) \sin(k_y y')]. \end{aligned}$$

We consider a design region shaped as a slab with infinite extent in the x direction and a thickness h in the y direction with the origin at the center. This is different from a half-space, but as we shall see the final result is completely independent of h and thus should apply in the limit $h \rightarrow \infty$. The different parities of cos and sin about the origin allow us to directly write down the

eigenvectors of $\text{Asym}\mathbb{G}_{k_x}$ as

$$|q_{\cos}(k_y)\rangle = \frac{\cos(k_y y)}{a_{\cos}}, \quad (\text{S68a})$$

$$|q_{\sin}(k_y)\rangle = \frac{\sin(k_y y)}{a_{\sin}} \quad (\text{S68b})$$

with normalization factor

$$a_{\cos}^2 = \int_{-h/2}^{h/2} \cos^2(k_y y) dy = \frac{1}{2k_y} (k_y h + \sin(k_y h)), \quad (\text{S68c})$$

$$a_{\sin}^2 = \int_{-h/2}^{h/2} \sin^2(k_y y) dy = \frac{1}{2k_y} (k_y h - \sin(k_y h)) \quad (\text{S68d})$$

and corresponding eigenvalues

$$\rho_{\cos}(k_y) = \frac{\tilde{k}^2}{2k_y} a_{\cos}^2, \quad (\text{S68e})$$

$$\rho_{\sin}(k_y) = \frac{\tilde{k}^2}{2k_y} a_{\sin}^2. \quad (\text{S68f})$$

We can thus write

$$\text{Asym}\mathbb{G}^{TM} = \int_{-\tilde{k}}^{\tilde{k}} dk_x \frac{e^{ik_x(x-x')}}{2\pi} \left(\rho_{\cos}(k_y) |q_{\cos}(k_y)\rangle \langle q_{\cos}(k_y)| + \rho_{\sin}(k_y) |q_{\sin}(k_y)\rangle \langle q_{\sin}(k_y)| \right). \quad (\text{S69})$$

The dipole source $\mathbf{J}(x', y') = \delta(x')\delta(y' - d - h/2)$ generates an incident field with the traveling wave components given by

$$\begin{aligned} \mathbf{E}_{v,travel}^{TM} &= -\frac{\tilde{k}}{2\sqrt{2\pi}} \int_{-\tilde{k}}^{\tilde{k}} dk_x \frac{e^{ik_x x}}{\sqrt{2\pi}} \frac{1}{k_y} e^{ik_y(d+h/2)} (\cos(k_y y) - i \sin(k_y y)), \\ -\mathbf{E}_{v,travel}^{TM*} &= \frac{\tilde{k}}{2\sqrt{2\pi}} \int_{-\tilde{k}}^{\tilde{k}} dk_x \frac{e^{ik_x x}}{\sqrt{2\pi}} \frac{1}{k_y} e^{-ik_y(d+h/2)} (\cos(k_y y) + i \sin(k_y y)). \end{aligned}$$

While $\text{Asym}\mathbb{G}$ is technically semi-definite, the incident field $\mathbf{E}_{v,travel}$ is contained completely in the span of the non-singular eigenvectors $q_{\cos}(k_y)$, $q_{\sin}(k_y)$. Thus we can write down $\text{Asym}\mathbb{G}^{-1} \cdot \mathbf{E}_{v,travel}$ as

$$\text{Asym}\mathbb{G}^{TM-1} \cdot \mathbf{E}_{v,travel}^{TM} = -\frac{\tilde{k}}{2\sqrt{2\pi}} \int_{-\tilde{k}}^{\tilde{k}} dk_x \frac{e^{ik_x x}}{\sqrt{2\pi}} \frac{1}{k_y} e^{ik_y(d+h/2)} (\rho_{\cos}^{-1} \cos(k_y y) - i \rho_{\sin}^{-1} \sin(k_y y)) \quad (\text{S70})$$

which can be formally interpreted as a pseudo-inverse or the inverse restricted to the relevant non-singular subspace. Thus we have

$$\begin{aligned} \langle \mathbf{E}_{v,travel}^{TM} | \text{Asym}\mathbb{G}^{TM-1} | \mathbf{E}_{v,travel}^{TM} \rangle &= \frac{\tilde{k}^2}{8\pi} \int_{-\tilde{k}}^{\tilde{k}} \frac{1}{k_y^2} \left(\frac{a_{\cos}^2}{\rho_{\cos}} + \frac{a_{\sin}^2}{\rho_{\sin}} \right) dk_x \\ &= \frac{\tilde{k}^2}{8\pi} \int_{-\tilde{k}}^{\tilde{k}} \frac{4}{\tilde{k}^2 k_y} dk_x \\ &= \frac{1}{2\pi} \int_{-\tilde{k}}^{\tilde{k}} \frac{1}{\sqrt{\tilde{k}^2 - k_x^2}} dk_x \\ &= \frac{1}{2}. \end{aligned} \quad (\text{S71})$$

A similar calculation yields

$$\begin{aligned} \langle -\mathbf{E}_{v,travel}^* | \text{Asym}\mathbb{G}^{-1} | \mathbf{E}_{v,travel} \rangle &= \frac{\tilde{k}^2}{8\pi} \int_{-\tilde{k}}^{\tilde{k}} \frac{e^{ik_y(2d+h)}}{k_y^2} \left(\frac{a_{cos}^2}{\rho_{cos}} - \frac{a_{sin}^2}{\rho_{sin}} \right) dk_x \\ &= 0. \end{aligned} \quad (\text{S72})$$

This gives the traveling wave contribution to the material-independent LDOS enhancement limits

$$\begin{aligned} \rho_{sca}^{TM} &= \frac{1}{4} \text{Re} \{ \langle -\mathbf{E}_{v,travel}^{TM*} | (\text{Asym}\mathbb{G}^{TM})^{-1} | \mathbf{E}_{v,travel}^{TM} \rangle \} + \frac{\tilde{k}}{4} \langle \mathbf{E}_{v,travel}^{TM} | (\text{Asym}\mathbb{G}^{TM})^{-1} | \mathbf{E}_{v,travel}^{TM} \rangle \\ &= \frac{\tilde{k}}{8}. \end{aligned} \quad (\text{S73})$$

Thus, if only the traveling waves (far field) are considered, $\rho_{sca}^{TM}/\rho_0^{TM}$ tends towards a constant value of 1 in the single frequency limit. This can indeed be observed in the numerics for narrow bandwidth and large separation d , where the near-field contribution has decayed exponentially to the point of being negligible. An analogous calculation for TE shows that there the ratio is 1/2.

11.1.2 Evanescent wave contribution

We evaluate the bandwidth scaling of the evanescent wave contribution for lossless materials ($\chi_i = 0$) and TM polarization. To do so, we choose the phase parameter $p = 1 + ip_i$ with the imaginary part $p_i \rightarrow 0$. As we shall see, this not only simplifies the asymptotic analysis for small bandwidth but also will lead to material independent bounds that are finite.

Given $\chi_i = 0$, we have the material factor $\lim_{p_i \rightarrow 0} \text{Im}\{p/\chi^*\} \rightarrow 0$. Furthermore, from (S57) we have

$$r_- \sim \sqrt{k_{yi}^2 - k_{yr}^2 - \frac{2k_{yr}k_{yi}(B_ik_{yi} - B_rk_{yr})}{B_rk_{yi} + B_ik_{yr}}} \quad r_+ \sim \sqrt{\frac{\chi(B_rk_{yi} + B_ik_{yr})}{p_i}} \quad p_i \rightarrow 0 \quad (\text{S74})$$

so we see that in the limit $p_i \rightarrow 0$, r_- tends toward a finite value while r_+ diverges $\propto p_i^{-1/2}$.

To simplify the analysis, we can use the Cauchy-Schwartz relaxed (S49) to get

$$\begin{aligned} \rho_{sca}^{TM} &\leq \frac{|\tilde{\omega}|}{2} \langle \mathbf{E}_v^{TM} | \text{Asym}(p\mathbb{U}^{TM})^{-1} | \mathbf{E}_v^{TM} \rangle \\ &= \frac{1}{8\pi} \int_0^\infty \text{Re} \left\{ \frac{|\tilde{k}|^3 e^{-2k_{yi}d}}{|k_y|^2} \left(\frac{R_+}{r_+ + ik_y^*} + \frac{R_-}{r_- + ik_y^*} \right) \right\} dk_x. \end{aligned} \quad (\text{S75})$$

Now, treating r_+ as a large variable in the limit $p_i \rightarrow 0$, asymptotic analysis of (S59) and (S61) gives

$$\frac{R_+}{r_+ + ik_y^*} + \frac{R_-}{r_- + ik_y^*} \sim \frac{8k_{yi}|k_y|^2}{\text{Im}\{p/\chi^*\}r_+^2 [(r_- + k_{yi})^2 + k_{yr}^2]} \quad p_i \rightarrow 0 \quad (\text{S76})$$

Since $\text{Im}\{p/\chi^*\} \propto p_i$ and $r_+^2 \propto p_i^{-1}$ in the limit p_i , we see that the entire integrand of (S75) tends toward a finite value

$$\rho_{sca}^{TM} \leq \frac{1}{8\pi} \int_0^\infty \text{Re} \left\{ |\tilde{k}|^3 e^{-2k_{yi}d} \frac{8k_{yi}}{(B_rk_{yi} + B_ik_{yr}) [(r_- + k_{yi})^2 + k_{yr}^2]} \right\} dk_x, \quad (\text{S77})$$

so the bound with $p = 1$ is well-defined. We can now consider the narrow bandwidth limit $\tilde{k}_i \rightarrow 0$ given $p = 1$. It has already been established that the traveling wave contribution from the $k_x < \tilde{k}_r$ part of the integrand is a constant in the narrow bandwidth limit. In the evanescent region $k_x > \tilde{k}_r$, to lowest order in \tilde{k}_i we have

$$k_{yi} \sim \sqrt{k_x^2 - \tilde{k}_r^2} \quad k_{yr} \sim \frac{\tilde{k}_r}{k_{yi}} \cdot \tilde{k}_i \quad \tilde{k}_i \rightarrow 0 \quad (\text{S78a})$$

$$B_i \sim -\frac{\tilde{k}_r^2}{k_{yi}} \quad B_r \sim \left(\frac{\tilde{k}_r^3}{k_{yi}^3} + \frac{2\tilde{k}_r}{k_{yi}} \right) \cdot \tilde{k}_i \quad \tilde{k}_i \rightarrow 0 \quad (\text{S78b})$$

$$r_-(p=1) \sim \sqrt{\tilde{k}_r^2 + k_{yi}^2} \quad \tilde{k}_i \rightarrow 0 \quad (\text{S78c})$$

All of these combine together to give

$$\text{Re} \left\{ \left| \tilde{k} \right|^3 e^{-2k_{yi}d} \frac{8k_{yi}}{(B_r k_{yi} + B_i k_{yr}) [(r_- + k_{yi})^2 + k_{yr}^2]} \right\} \propto \tilde{k}_i^{-1} \quad k_x > \tilde{k}_r, \tilde{k}_i \rightarrow 0 \quad (\text{S79})$$

and we see that the evanescent wave contribution gives the inverse bandwidth scaling for lossless materials, as seen in the main text.

11.2 TM material Scaling

From section 11.1.2 we see that given lossless χ the bound with $p = 1$ is finite and well-defined, amounting to

$$\rho_{sca}^{TM} \leq \frac{\tilde{\omega}}{2} \langle \mathbf{E}_v^{TM} | \text{AsymG}^{TM-1} | \mathbf{E}_v^{TM} \rangle, \quad (\text{S80})$$

which is a bound independent of χ , and thus therefore applies to all lossless χ . The next step is to show that (S80) is also a bound for lossy χ with $\text{Im}(\chi) > 0$. We can see this by again setting $p = 1$ in (S48) and applying the Cauchy-Schwartz inequality to arrive at a bound for lossy χ :

$$\rho_{sca}^{TM} \leq \frac{|\tilde{\omega}|}{2} \langle \mathbf{E}_v^{TM} | \left(\frac{\chi_i}{|\chi|^2} + \text{AsymG}^{TM} \right)^{-1} | \mathbf{E}_v^{TM} \rangle. \quad (\text{S81})$$

Now as operators we have $\frac{\chi_i}{|\chi|^2} \succ 0$ and $\text{AsymG}^{TM} \succeq 0$, so $\langle \mathbf{E}_v^{TM} | \left(\frac{\chi_i}{|\chi|^2} + \text{AsymG}^{TM} \right)^{-1} | \mathbf{E}_v^{TM} \rangle < \langle \mathbf{E}_v^{TM} | \text{AsymG}^{TM-1} | \mathbf{E}_v^{TM} \rangle$ and it is clear that the material independent bound (S80) while derived assuming $\chi_i = 0$ applies to general lossy χ . Thus in general as $|\chi| \rightarrow \infty$, the TM halfspace LDOS limits do not diverge, but are always bounded by (S80).

11.3 TM separation scaling

In this section we investigate the scaling of the TM half-space bounds with the vacuum separation d as $d \rightarrow 0$. The k_x integral in (S75) converges for finite d due to the exponential decay factor $e^{-2k_{yi}d}$: as $k_x \rightarrow \infty$, $k_{yi} \approx k_x \rightarrow \infty$. The scaling of (S75) with d thus depends on the k_x scaling of the rest of the integrand as $k_x \rightarrow \infty$.

11.3.1 Finite χ

Given finite χ , we can always select a complex phase p such that $\text{Im}\{p/\chi^*\} > 0$. Now from (S43b) and (S78a) it is clear that $\lim_{k_x \rightarrow \infty} \text{Asym}(p\mathbb{U}^{TM})_{k_x} = \text{Im}\{p/\chi^*\}$, since $\lim_{k_x \rightarrow \infty} \tilde{k}^2/k_y = 0$ and $\lim_{k_x \rightarrow \infty} e^{ik_y|y-y'|} \rightarrow 0$ for $y \neq y'$ (if $y = y'$ then $e^{ik_y|y-y'|} = 1$ but this is a finite non-zero value of the integral kernel with support over a set of measure 0 and the integral operator as a whole still goes to 0).

The k_x integrand of $\langle \mathbf{E}_v^{TM} | \text{Asym}(p\mathbb{U}^{TM})^{-1} | \mathbf{E}_v^{TM} \rangle$ given in (S44) for large k_x is then approximately

$$\frac{e^{-2k_x d}}{k_x^2} \text{Im}\{p/\chi^*\}^{-1} \int_0^\infty e^{-2k_x y} dy \propto \frac{e^{-2k_x d}}{k_x^3}.$$

Even at exactly $d = 0$, the integrand scales $\propto k_x^{-3}$ as $k_x \rightarrow \infty$ and the integral converges. Thus for finite χ the half-space LDOS bounds approach a finite constant as $d \rightarrow 0$.

11.3.2 Material independent bounds

For the material independent bound given in (S80), the k_x integrand is given by (S77) and (S78). In the narrow-bandwidth, large k_x limit the integrand

$$\text{Re} \left\{ \left| \tilde{k} \right|^3 e^{-2k_{yi}d} \frac{8k_{yi}}{(B_r k_{yi} + B_i k_{yr}) [(r_- + k_{yi})^2 + k_{yr}^2]} \right\} \sim \frac{\left| \tilde{k} \right|^3}{k_r} \frac{1}{k_i} \frac{e^{-2k_x d}}{k_x} \quad k_i \rightarrow 0, k_x \rightarrow \infty \quad k_x \rightarrow \infty. \quad (\text{S82})$$

Thus the material independent bound scaling as $d \rightarrow 0$ can be evaluated as

$$\begin{aligned} \rho_{sca, max}^{TM} &\sim \frac{1}{8\pi} \frac{\left| \tilde{k} \right|^3}{k_r} \frac{1}{k_i} \int_{\beta \tilde{k}_r}^\infty \frac{e^{-2k_x d}}{k_x} dk_x \\ &= \frac{1}{8\pi} \frac{\left| \tilde{k} \right|^3}{k_r} \frac{1}{k_i} E_1(2\beta \tilde{k}_r d) \\ &\sim \frac{1}{8\pi} \frac{\left| \tilde{k} \right|^3}{k_r} \frac{1}{k_i} \ln(\lambda_0/d) \end{aligned} \quad (\text{S83})$$

where we have selected a constant $\beta \gg 1$ such that the large k_x approximations hold; as seen in (S83) the exact value of β is irrelevant to the leading order asymptotic of $\ln(1/d)$. Note that this is a different scaling than the finite χ bounds in the previous subsection. A consequence of the material independent bounds diverging whilst fixed material bounds saturating as $d \rightarrow 0$ is that smaller d increases the relative advantage of large materials, as seen in Fig. (2b) in the main text.

11.4 TE separation scaling

The prior sections on the asymptotics of the TM case have demonstrated scaling of the bounds with the inverse of the bandwidth (for lossless materials) and saturation with increasing material susceptibility; the TE bounds share these scaling characteristics so for the sake of simplicity we will not do a detailed TE asymptotic analysis.

However, there is a difference in the $d \rightarrow 0$ scaling between the TM and TE results, which can be understood by comparing the $k_x \rightarrow \infty$ characteristics of \mathbf{E}_{v,k_x}^{TM} and \mathbf{E}_{v,k_x}^{TEy} . For TE, we have

$$\begin{aligned}
\rho_{sca}^{TEy} &\leq 2 \int_0^\infty \left\langle \mathbf{E}_{v,k_x}^{TEy} \middle| \text{Asym}(p\mathbb{U}_{k_x}^{TE})^{-1} \middle| \mathbf{E}_{v,k_x}^{TEy} \right\rangle dk_x \\
&= 2 \int_0^\infty \left\langle \mathbf{E}_{v,k_x}^{TEy} \middle| (\text{Im}\{p/\chi^*\} + \text{Asym}(p^*\mathbb{G}_{k_x}^{TE}))^{-1} \middle| \mathbf{E}_{v,k_x}^{TEy} \right\rangle dk_x \\
&< 2 \int_0^\infty \text{Im}\{p/\chi^*\}^{-1} \|\mathbf{E}_{v,k_x}^{TEy}\|^2 dk_x \\
&= \frac{1}{4\pi|\tilde{k}|^2} \int_0^\infty \frac{e^{-2k_y d}}{2k_{yi}} \left(k_x^2 + \frac{k_x^4}{|k_y|^2} \right) dk_x.
\end{aligned}$$

In the $k_x \rightarrow \infty$ limit, the integrand $\sim k_x e^{-2k_x d}$, so similar to (11.3.1), for the $d \rightarrow 0$ asymptotics we have

$$\begin{aligned}
\rho_{sca}^{TEy} &\lesssim \frac{1}{4\pi|\tilde{k}|^2} \int_{\beta\tilde{k}_r}^\infty k_x e^{-2k_x d} dk_x \quad d \rightarrow 0 \\
&= \frac{1}{d^2} \frac{1}{4\pi|\tilde{k}|^2} \cdot \frac{1}{4} e^{-2\beta\tilde{k}_r d} (2\beta\tilde{k}_r d + 1) \quad d \rightarrow 0 \\
&\propto \frac{1}{d^2} \quad d \rightarrow 0
\end{aligned} \tag{S84}$$

and we recover the $1/d^2$ scaling of the TE bounds seen in the main text.

11.4.1 3D separation scaling

For a point dipole near a 3D half-space design region, a similar analysis would yield $1/d^3$ scaling of the LDOS bounds. Due to the extra spatial dimension as compared with the TE case, the 1D k_x integral becomes a 2D k_\parallel integral. For simplicity, suppose that the dipole is aligned with the normal of the design region surface, giving the problem cylindrical symmetry. The spatial integration kernel is then $2\pi \int_0^\infty k_\parallel(\cdot) dk_\parallel$, with the bound integral analogous to (S84) having an extra k_\parallel factor in the integrand. This will lead to $\propto 1/d^3$ scaling, as seen in [5].

12 Comparison to passivity bounds

The main prior work concerning finite bandwidth LDOS limits is [5], where an bound based on passivity constraints was derived:

$$\rho_{sca} \leq \frac{|\tilde{\omega}|}{2} f(\tilde{\omega}, \chi) \langle \mathbf{E}_v | \mathbf{E}_v \rangle \tag{S85a}$$

with the material figure of merit

$$f(\tilde{\omega}, \chi) = \frac{|\tilde{\omega}\chi|^2 + |\tilde{\omega}\chi|\Delta\tilde{\omega}}{|\tilde{\omega}|\text{Im}(\tilde{\omega}(1+\chi))}. \tag{S85b}$$

Note that compared to (22) in [5], we have dropped the electrostatic contribution (as in the main text), and there is an additional factor of $\pi|\tilde{\omega}|^2$ due to differences in definitions (the π factor is a matter of convention; the $|\tilde{\omega}|^2$ factor comes from \mathbf{E}_v in our work coming from a unit amplitude dipolar current source instead of a unit dipole moment). Compared to the material bound given by (16) in the main text, (S85) essentially corresponds to a particular value of p . For example, given a lossless χ and narrow bandwidth $\Delta\omega \ll |\tilde{\omega}|$, we have

$$f(\tilde{\omega}, \chi) \approx \frac{|\tilde{\omega}|}{\Delta\omega} \frac{\chi^2}{1 + \chi}.$$

Now if we select a phase rotation p such that $p_r = 1$,

$$p_i = \frac{\chi + 1}{\chi} \frac{\Delta\omega}{|\tilde{\omega}|}, \quad (\text{S86})$$

the material bound is

$$\frac{|\tilde{\omega}|}{2} \text{Im}\{p/\chi^*\}^{-1} \langle \mathbf{E}_v | \mathbf{E}_v \rangle = \frac{|\tilde{\omega}|}{2} \frac{|\tilde{\omega}|}{\Delta\omega} \frac{\chi^2}{1 + \chi} \langle \mathbf{E}_v | \mathbf{E}_v \rangle = \frac{|\tilde{\omega}|}{2} f(\tilde{\omega}, \chi) \langle \mathbf{E}_v | \mathbf{E}_v \rangle$$

which is exactly equivalent to the passivity bound. Checking (S39) it is clear that with such a phase rotation p , $\text{Asym}(p\mathbb{U})$ remains positive definite.

12.1 Bandwidth scaling of the passivity bounds

The passivity bounds (S85) have increased bandwidth scaling given an infinite halfspace design region coming from traveling wave contributions to $\langle \mathbf{E}_v | \mathbf{E}_v \rangle$. For example, given TM polarization we have

$$\begin{aligned} \langle \mathbf{E}_v^{TM} | \mathbf{E}_v^{TM} \rangle &= \frac{|\tilde{k}|^2}{8\pi} \int_{-\infty}^{\infty} \frac{e^{-2k_{yi}d}}{|k_y|^2} \int_0^{\infty} e^{-2k_{yi}y} dy dk_x \\ &= \frac{|\tilde{k}|^2}{8\pi} \int_{-\infty}^{\infty} \frac{e^{-2k_{yi}d}}{2|k_y|^2 k_{yi}} dk_x. \end{aligned}$$

Now for traveling waves $|k_x| < \tilde{k}_r$, it can easily be shown from $k_y = \sqrt{\tilde{k}^2 - k_x^2}$ that $k_{yi} \propto \tilde{k}_i$, leading to $\langle \mathbf{E}_v^{TM} | \mathbf{E}_v^{TM} \rangle \propto 1/\tilde{k}_i \propto 1/\Delta\omega$ (this analysis also applies to TE polarization). For lossless dielectrics, $f(\tilde{\omega}, \chi) \approx \frac{|\tilde{\omega}|}{\Delta\omega}$, giving the passivity bounds an overall $1/\Delta\omega^2$ scaling, as compared to the $1/\Delta\omega$ scaling for the full bounds. For lossy materials $f(\tilde{\omega}, \chi) \approx \frac{|\chi|^2}{\chi_i}$, giving the passivity bounds an overall $1/\Delta\omega$ scaling, as compared to the $1/\Delta\omega^4$ scaling of the full bounds seen in Fig (3) of the main text.

References

- [1] Tyler W Hughes, Ian AD Williamson, Momchil Minkov, and Shanhui Fan. Forward-mode differentiation of Maxwell's equations. *ACS Photonics*, 6(11):3010–3016, 2019.
- [2] S. G. Johnson et al. *The NLOpt Nonlinear Optimization Package (Version 2.6.2)*. August 2019.

- [3] Sean Molesky, Pengning Chao, and Alejandro W. Rodriguez. Hierarchical mean-field \mathbb{T} operator bounds on electromagnetic scattering: Upper bounds on near-field radiative Purcell enhancement. *Physical Review Research*, 2(4):043398, December 2020.
- [4] Walter Rudin. *Real and Complex Analysis*. McGraw-Hill Education, New York, 2006.
- [5] Hyunki Shim, Lingling Fan, Steven G. Johnson, and Owen D. Miller. Fundamental Limits to Near-Field Optical Response over Any Bandwidth. *Physical Review X*, 9(1):011043, March 2019.
- [6] Leung Tsang, Jin Au Kong, and Kung-Hau Ding. *Scattering of Electromagnetic Waves: Theories and Applications*, volume 27. John Wiley & Sons, 2004.